The International Journal of Advanced Manufacturing Technology (2018) 95:3413–3435
https://doi.org/10.1007/s00170-017-1385-8

ORIGINAL ARTICLE

Prediction and compensation of geometric error for translational axes in multi-axis machine tools

Changjun Wu[1,2] · Jinwei Fan[1] · Qiaohua Wang[2] · Ri Pan[1] · Yuhang Tang[1] · Zhongsheng Li[1]

Received: 30 July 2017 / Accepted: 13 November 2017 / Published online: 11 December 2017

Abstract
This paper proposes an integrated geometric error prediction and compensation method to eliminate the positioning inaccuracy of tool ball for a double ball bar (DBB) caused by the translational axes' geometric errors in a multi-axis machine tool (MAMT). Firstly, based on homogeneous transform matrix (HTM) and multi-body system (MBS) theory, the positioning error model only considering the translational axes of a MAMT is established. Then, an integrated error parameter identification method (IEPIM) by using a laser interferometer is proposed. Meanwhile, the identification discrete results of geometric error parameters for the translational axes are obtained by identification experiments. According to the discrete values, the optimal polynomials of 18 position-dependent geometric errors (PDGEs) are founded. As a basis, an iterative compensation method is constructed to modify the NC codes generated with the ordinary compensation method in self-developed compensation software. Finally, simulation verification is conducted with these two compensation methods. Simulation results show the positioning errors for test path of tool ball calculated with the iterative compensation method that are limited within 0.001 mm, and its average accuracy and accuracy stability are improved by 79.5 and 52.2%, respectively. In order to further verify the feasibility of the presented method, a measuring experiment is carried out in *XY* plane of a five-axis machine tool by using DBB. The experiment results show that the maximum circularity error with the iterative compensation method is reduced about 40.4% than that with the ordinary compensation method. It is therefore reasonable to conclude that the proposed method in this paper can avoid the influence of the translational axes' geometric errors on rotary ones during a DBB test.

Keywords Translational axes · Geometric error · Positioning error · Integrated error parameter identification method · Iterative compensation method · The optimal polynomials

1 Introduction

With a rapid development of precision machining for the complex parts, multi-axis machine tools (MAMTs) are preferred with the advantages of higher material removal rate and better ability of positioning and orienting the tool with respect to the workpiece and lower production cost [1–3]. Nevertheless, current MAMTs cannot offer the same machining accuracy as their three-axis counterparts. This hinders the wider acceptance and practical implementation of MAMTs. It is obvious that major obstacles are that the introduction of rotary axes radically changes the machine's kinematic structure and brings in more error sources.

Recently, many researchers have investigated some measuring pattern to identify the rotary axes' geometric errors, which are the key contributors resulting in poor machining accuracy of machine tools [4]. Tsutsumi et al. [5] presented a measuring method for each rotary axis to identify the particular deviations based on simultaneous three-axis control motions by using the double ball bar (DBB). Lee et al. [6] estimated geometric errors for a rotary axis using DBB and assumed that all of the geometric errors for the translational axes were compensated and negligible. Lee et al. [7] designed four measurement paths to identify position-independent

✉ Changjun Wu
piaoyanggh2003@163.com

✉ Jinwei Fan
jwfan@bjut.edu.cn

[1] College of Mechanical Engineering & Applied Electronics Technology, Beijing University of Technology, Beijing 100124, People's Republic of China

[2] School of Mechanical and Electrical Engineering, Zhengzhou University of Light Industry, Zhengzhou 450002, People's Republic of China

geometric errors of rotary axes *A* and *C* of a five-axis machine tool using a DBB and assumed that the positioning accuracies of the translational axes were within tolerances. Chen et al. [3] proposed seven measurement patterns of multi-axis synchronous movement to predict and identify the rotary axes *B* and *C* of a non-orthogonal five-axis machining center using the DBB. Chen et al. [8] proposed a comprehensive geometric error measurement and identification method for a tilt table of a five-axis machine tool by using DBB on the basis of the assumption that the geometric errors of the translational axes were ignored during the experiments.

However, the measurement of the rotary axes is usually realized by detecting position changes of two ends of the DBB (i.e., worktable end and cutting tool end), which are driven by the multi-axis synchronous motion. The assumption that geometric errors caused by the translational axes have been compensated perfectly will result in the positioning inaccuracy of two ends of the DBB and affect the measuring results of rotary axes, thus reducing machining accuracy of MAMTs.

According to ref. [9], the positioning inaccuracy of worktable end for DBB caused by the errors of the translational axes can be avoided. Nevertheless, to the best of our knowledge, the positioning inaccuracy of cutting tool end for DBB caused by the errors of the translational axes is rarely noticed.

Hence, in order to eliminate the influence of the translational axes' errors on the rotary ones, positioning inaccuracy of cutting tool end for DBB caused by the translational axes' errors should be compensated in real time during the measurement experiment of the rotary axes.

Hsu et al. [10] divided the error compensation techniques into three steps: (1) using a measuring device to measure errors, (2) developing an error model for machine tools, and (3) carrying out error compensation by using the obtained errors and the established error model. So, the measurement and identification of error sources are the prerequisite to set up error model and conduct error compensation.

Over the past few decades, many literatures have reported the geometric errors identification methods for translational axes, mainly including identification method of individual error measurement (IDOIEM) and integrated error parameter identification method (IEPIM) [2, 11–13]. For the IDOIEM, only one error component can be measured at one time and various special measurement instruments are used to measure and identify different types of error parameters. In addition, the method requires familiarity with measurement instruments and operator experts. For these reasons, the measurement efficiency is very low, and the measurement task is very tedious and laborious. Comparatively speaking, the IEPIM has been well recognized in a large amount of research due to many advantages, such as faster measuring speed, higher measurement precision, simpler operation, and fewer measurement instruments.

Among the measurement instruments utilized by the IEPIM, the laser interferometer is gradually becoming widely used in machine tool industry since it is a heterodyne interferometry technology based on Doppler shift, with high resolution, high precision, and quick response characters [14, 15]. However, some drawbacks still exist in these IEPIMs based on the laser interferometer. Zhang et al. [16] proposed a 22-line method to obtain the geometric error components of a three-axis machine tool. But the method can only be solved by cycle or traversal algorithm and has a strict requirement regarding measuring points, which make the method difficult to implement and lack intuition. Liu [17] and Fan et al. [18] developed the 9-line method and 14-line method to identify geometric error parameter of three translational axes of a machine tool by using the laser interferometer, respectively. But, the low identification accuracy in the 9-line method and the assumption that all straightness errors have a 0 sum in the 14-line method make them lack universal property. Chen [19] and Su et al. [20] presented the 15-line method and 12-line method, respectively. But, these two methods ignore the influence of translational motion errors on the straightness errors, which decrease the identification accuracy. Based on the aforementioned methods, Li et al. [21] summarized their characteristics and proposed a novel 13-line method based on a laser interferometer. But, the identification process of the method is complex and time consuming and the division of subspaces is likely to give rise to the error accumulation, which reduce the identification efficiency and accuracy.

According to the refs. [21–25], error compensation is divided into hardware compensation and software compensation. Generally speaking, hardware compensation is not recommended since machining costs rise exponentially with the level of machining accuracy involved [21, 23], whereas software compensation does not need to take into account economic limitations since only a computer software is needed to compensate errors by correcting numerical control (NC) instructions before executing compensation instructions [22, 24, 25]. Therefore, in this study, software compensation is chosen to be used.

In order to carry out software compensation perfectly, a systematic and suitable error modeling method should be applied [26]. As a modeling method that can describe the motion relationship between the adjacent kinematic parts of machine tools simply and conveniently based on homogeneous transform matrix (HTM) [27, 28], multi-body system (MBS) is the most widely utilized way. Fan et al. [29] proposed a generalized kinematics error modeling method to improve the machining accuracy of NC machine tools by error compensation based on MBS. To date, just as Zhu et al. [30] indicate, it is the best method for geometric error modeling of machine tools.

It is worth noting that error parameters of machine tools with the characteristics of nonlinearity and uncertainty, obtained by measurement and identification techniques, are the

discrete values related to the position [31]. However, in the process of error modeling and error compensation, the discrete data cannot be directly used because they are not feasible enough to provide necessary information at an arbitrary position, thus having influence on software compensation effect. Therefore, error parameters models need to be developed to compute error values at any position. In some references, position-dependent geometric error (PDGE) parameters are modeled by various functions, such as first-order polynomials (Jung et al. [32]), Fourier series (Bringmann et al. [33]), cubic polynomials (Lasemi et al. [34]), and fifth-order polynomials (Huang et al. [35]). Although these error parameters models have been proved to be effective, they cannot provide sufficient accuracy to describe the error behavior. Lee et al. [36] developed the analytical polynomials of geometric error components whose orders were determined by inspecting the mean square error (MSE) of the residual errors. However, according to the ref. [37], the individual error is variational and stochastic. If the terms of the polynomial are too large, the mathematical error models are difficult to be utilized since it leads to too much calculation during the error compensation process. In addition, if the polynomial includes the terms having little influence on PDGE, its prediction accuracy will be affected. And if the polynomial ignores the terms having a significant influence on error, then the error models have a great deviation from the actual ones, which will make the polynomial meaningless. Therefore, how to establish the optimal models of geometric error parameters is of paramount importance.

In view of the limitations stated, first, this paper presents a general IEPIM to measure and identify the geometric errors of translational axes in MAMTs. In order to predict the error information at an arbitrary position effectively, the optimal models of geometric error parameters are established to represent the non-linear relations between the axis position and the geometric errors. Finally, a software compensation method is developed to attain the desired positioning accuracy at the end of cutting tool. This paper is organized as follows: positioning error prediction model is established in Sect. 2. The measurement and identification method of geometric errors for translational axes related to one type MAMTs are presented in Sect. 3. In Sect. 4, the geometric error identification experiment and the modeling process of geometric error parameters are described. A software compensation method of geometric error, the simulation verification, and a test experiment are presented in Sect. 5. And finally, some conclusions are drawn in Sect. 6.

2 Positioning error modeling

2.1 Structure of the MAMT

An investigated MAMT is shown in Fig. 1a. Based on MBS theory, the machine tool can be considered as the combination of various rigid bodies, including machine bed (body 1), *Y* axis slide carriage (body 2), *C* axis (i.e., worktable, body 3), workpiece (body 4), *X* axis slide carriage (body 5), *Z* axis slide carriage (body 6), *B* axis (body 7), tool spindle (body 8), and cutting tool (body 9). Furthermore, in Fig. 1a, the ball of worktable end for DBB is called as workpiece ball, and the ball of cutting tool end is called as tool ball.

Since this paper aims at the translational axes of the MAMT, its kinematic chain (as shown in Fig. 1b) is figured out by fixing *C* axis and *B* axis as one unit moving with the *Z* axis and *Y* axis, respectively. In addition, according to the lower body array approach [18], its topology structure map is established, as shown in Fig. 2.

2.2 Geometric error parameter definition and setting of the coordinate systems

Geometric errors of machine tools are usually classified into position-dependent geometric errors (PDGEs) and position-independent geometric errors (PIGEs) [12, 34]. PDGEs change with the moving position of the axis. On the other hand, PIGEs always keep constant [38].

According to ISO230-1 [39], three translational axes of a MAMT have a total of 21 geometric error parameters, i.e., 18 PDGEs (six errors for each axis) and 3 PIGEs. Figure 3a is the schematic diagram of *Y* axis PDGEs, and Fig. 3b is the schematic diagram of PIGEs between translational axes, where $\delta_i(y)$ and $\varepsilon_i(y)$ $(i = x, y, z)$ represent PDGEs of *Y* axis along the *i* direction, respectively, while ε_{xy}, ε_{yz}, and ε_{xz} denote the PIGE of between *X* and *Y*, *Y* and *Z*, *X* and *Z*, respectively. Table 1 shows all the geometric errors of the translational axes for the MAMT.

For the convenience of this study, some hypotheses are made as follows: (1) the machine coordinate system (MCS) $O_M - X_M Y_M Z_M$ is selected as the base coordinate system (BCS). Moreover, the coordinate system of bodies 1 and 2 and the BCS are in the same direction. (2) The ideal coordinate system direction of each body is in line with the BCS. (3) The coordinate system $O_W - X_W Y_W Z_W$ is selected as workpiece coordinate system (WCS), whose origin is set at the geometrical center point O_W of end surface in body 3. In addition, the coordinate system $O_T - X_T Y_T Z_T$ is selected as tool coordinate system (TCS), whose origin is set at the intersection point O_T of the axis center line in bodies 7 and 9, as shown in Fig. 1a.

2.3 Positioning error modeling

When the translational axes of the MAMT is only taken into account, the relative motion path variation of the tool ball with respect to the workpiece ball can be regarded as the mere result caused by geometric errors of the translational axes.

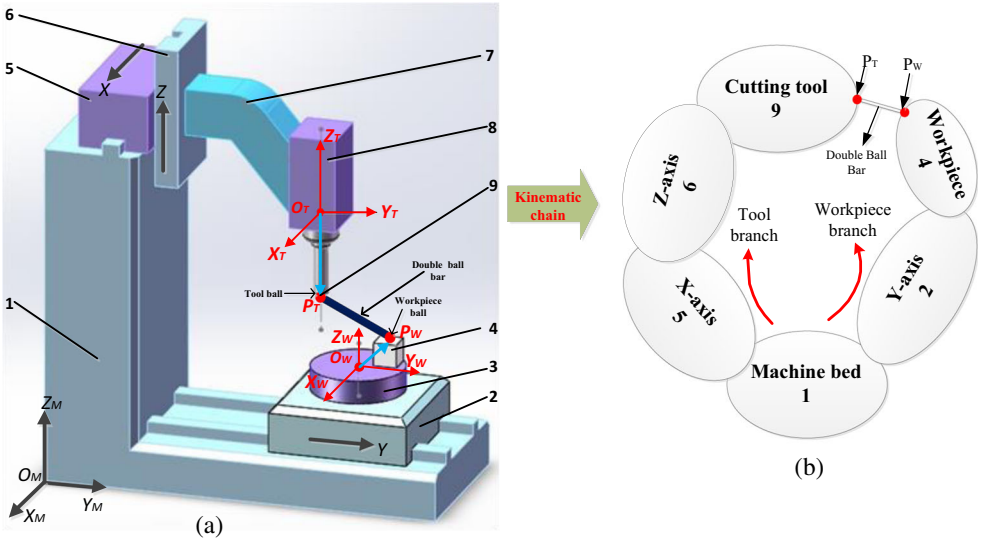

Fig. 1 A MAMT used in this research. **a** Structure. **b** Kinematic chain

Suppose that at the home position, the coordinate of O_W and O_T in the MCS can be written as $(q_{wx}\, q_{wy}\, q_{wz}\, 1)^T$ and $\left(q_{T_x} q_{T_y} q_{T_z}\, 1\right)^T$ respectively. The coordinate of the tool ball center point P_T in TCS can be expressed as $P_T = (X_T\, Y_T\, Z_T\, 1)^T$.

By utilizing MBS theory, the transformation matrix of the relative movement between the two adjacent bodies can be represented as

$$[SIJ] = [SIJ]_p[SIJ]_{pe}[SIJ]_s[SIJ]_{se} \tag{1}$$

where $[SIJ]_p$, $[SIJ]_{pe}$, $[SIJ]_s$, and $[SIJ]_{se}$ denote the relative position transformation matrix, the relative position error transformation matrix, the relative motion transformation matrix, the relative motion error transformation matrix between the rigid body I and the adjacent lower body J respectively.

According to Sect. 2.1, C axis is fixed on the Y axis. And B axis and the spindle are fixed on the Z axis. Therefore, the transformation matrix $[S24]$ between Y axis and workpiece and the transformation matrix $[S69]$ between Z axis and cutting tool can be obtained, respectively. Based on the abovementioned analysis, all of transformation matrices of the adjacent bodies can also be determined, as shown in Table 2.

As is seen in Fig. 2, the actual transformation matrix from body 1 to body 4, which is denoted as $[SBW]$, and the actual transformation matrix from body 1 to body 9, which is denoted as $[SBT]$, can be expressed in Eqs.(2) and (3) respectively.

$$\begin{aligned}[SBW] &= \prod_{t=n,L^n(3)=1}^{t=1}\left([SL^t(j)L^{t-1}(j)]_p[SL^t(j)L^{t-1}(j)]_{pe}[SL^t(j)L^{t-1}(j)]_s[SL^t(j)L^{t-1}(j)]_{se}\right)\\ &= [S12]_p[S12]_{pe}[S12]_s[S12]_{se}[S24]_p[S24]_{pe}[S24]_s[S24]_{se}\end{aligned} \tag{2}$$

$$\begin{aligned}[SBT] &= \prod_{t=n,L^n(4)=1}^{t=1}\left([SL^t(j)L^{t-1}(j)]_p[SL^t(j)L^{t-1}(j)]_{pe}[SL^t(j)L^{t-1}(j)]_s[SL^t(j)L^{t-1}(j)]_{se}\right)\\ &= [S15]_p[S15]_{pe}[S15]_s[S15]_{se}[S56]_p[S56]_{pe}[S56]_s[S56]_{se}[S69]_p[S69]_{pe}[S69]_s[S69]_{se}\end{aligned} \tag{3}$$

Since the point P_T in TCS can be described to WCS, the following equation is obtained.

$$P_T^W = [SBW]^{-1}[SBT]P_T \tag{4}$$

where P_T^W denotes the coordinate of the point P_T in WCS.

Assume that the coordinate of the workpiece ball center point in WCS can be expressed as $P_w = (x_w\, y_w\, z_w\, 1)^T$. Then, as shown in Fig. 4, the relative motion path vector between two ends of DBB P_E can be obtained as follows.

$$P_E = P_T^W - P_W = \begin{bmatrix} P_{E_x} \\ P_{E_y} \\ P_{E_z} \\ 0 \end{bmatrix} \tag{5}$$

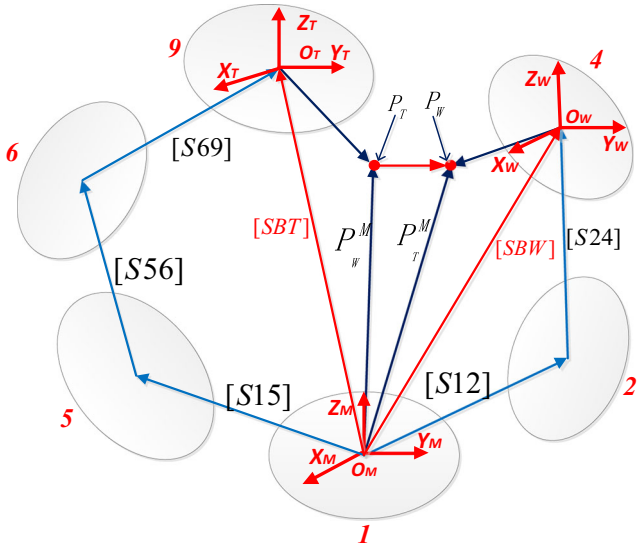

Fig. 2 The topology structure of the MAMT

where P_{E_x}, P_{E_y}, and P_{E_z} denote the component of P_E in x, y, z directions, respectively.

Therefore, the positioning error E can be obtained as follows.

$$\begin{cases} E = \sqrt{P_{E_x}^2 + P_{E_y}^2 + P_{E_z}^2} - l_1 \\ E_v = \begin{bmatrix} E_x \\ E_y \\ E_z \\ 1 \end{bmatrix} = \begin{bmatrix} E\cos\alpha \\ E\cos\beta \\ E\cos\gamma \\ 1 \end{bmatrix} \end{cases} \tag{6}$$

where E denotes the positioning error size. E_v denotes the coordinate vector of the positioning error. E_x, E_y, and E_z denote the component of E_v in x, y, z directions, respectively. l_1 denotes the ideal length of the ball bar. $\cos\alpha = P_{E_x}/\sqrt{P_{E_x}^2 + P_{E_y}^2 + P_{E_z}^2}$, $\cos\beta = P_{E_y}/\sqrt{P_{E_x}^2 + P_{E_y}^2 + P_{E_z}^2}$, and $\cos\gamma = P_{E_z}/\sqrt{P_{E_x}^2 + P_{E_y}^2 + P_{E_z}^2}$.

Table 1 Geometric errors of the translational axes for the MAMT

			X axis	*Y* axis	*Z* axis
PDGEs	Positioning error		$\delta_x(x)$	$\delta_y(y)$	$\delta_z(z)$
	Straightness error	x direction		$\delta_x(y)$	$\delta_x(z)$
		y direction	$\delta_y(x)$		$\delta_y(z)$
		z direction	$\delta_z(x)$	$\delta_z(y)$	
	Roll error		$\varepsilon_x(x)$	$\varepsilon_y(y)$	$\varepsilon_z(z)$
	Pitch error		$\varepsilon_y(x)$	$\varepsilon_x(y)$	$\varepsilon_x(z)$
	Yaw error		$\varepsilon_z(x)$	$\varepsilon_z(y)$	$\varepsilon_y(y)$
PIGEs	*XY* axis perpendicularity error		ε_{xy}		
	XZ axis perpendicularity error		ε_{xz}		
	YZ axis perpendicularity error		ε_{yz}		

3 The IEPIM of geometric error parameters

3.1 Multi-body synchronous motion modeling

As is seen in Fig. 1b, the three translational axes for the selected MAMT exist in different branches. *X* and *Y* axes can move with respect to machine bed. Moreover, *Z* axis can move with respect to *X* axis. Without loss of generality, machine bed and *X*, *Y*, and *Z* axes can be called as bodies *I*, *L*, *J* and *K* respectively. The schematic diagram of multi-body synchronous motion in different branches is shown in Fig. 5. Where $q_i^l, q_i^e, q_i (i = L, J, K)$ denote the ideal position vector, position error vector, and actual position vector of body i relative to the adjacent lower body, respectively. $S_{ih}^l, S_{ih}^e, S_{ih}$ $(i = L, J, K)$ denote the ideal motion vector, motion error vector, and actual motion vector of body i relative to the adjacent lower body when body i moves to the *h-th* $(h = 0,1,\ldots n)$ given position, respectively. $O_i - X_iY_iZ_i (i = I, L, J, K)$ represents the reference coordinate system of body i. n denotes the discrete point number.

Suppose at the hth given position, the position array of P_l for body L in the reference coordinate system of body L and I can be written as $\{r_l\} = \{r_{lx}\, r_{ly}\, r_{lz}\, 1\}^T$ and

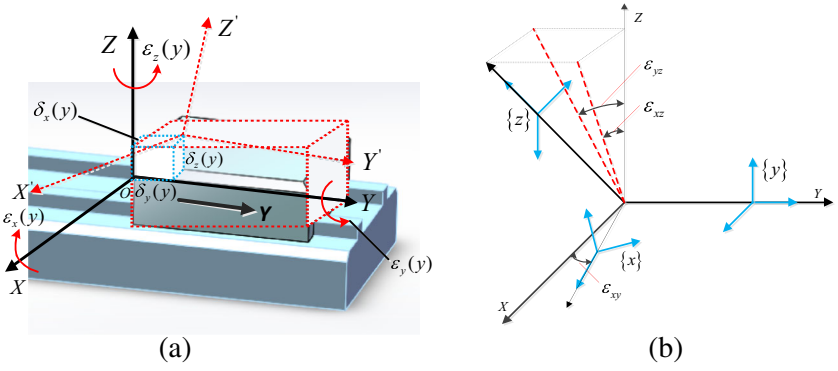

Fig. 3 The schematic diagram of geometric errors. **a** *Y* axis PDGEs. **b** PIGEs between translational axes

Table 2 Transformation matrix of the adjacent bodies for the researched machine tool

Adjacent body	Transformation matrix		Error transformation matrix	
	Position	Motion	Position	Motion
1–2 *Y* axis	$[S12]_p = I_{4\times4}$	$[S12]_s = \begin{bmatrix} 1 & 0 & 0 & 0 \\ 0 & 1 & 0 & y \\ 0 & 0 & 1 & 0 \\ 0 & 0 & 0 & 0 \end{bmatrix}$	$[S12]_{pe} = I_{4\times4}$	$[S12]_{se} = \begin{bmatrix} 1 & -\varepsilon_z(y) & \varepsilon_y(y) & \delta_x(y) \\ \varepsilon_z(y) & 1 & -\varepsilon_x(y) & \delta_y(y) \\ -\varepsilon_y(y) & \varepsilon_x(y) & 1 & \delta_z(y) \\ 0 & 0 & 0 & 1 \end{bmatrix}$
2–4 workpiece	$[S24]_p = \begin{bmatrix} 1 & 0 & 0 & q_{wx} \\ 0 & 1 & 0 & q_{wy} \\ 0 & 0 & 1 & q_{wz} \\ 0 & 0 & 0 & 1 \end{bmatrix}$	$[S24]_s = I_{4\times4}$	$[S24]_{pe} = I_{4\times4}$	$[S24]_{se} = I_{4\times4}$
1–5 *X* axis	$[S15]_p = I_{4\times4}$	$[S15]_s = \begin{bmatrix} 1 & 0 & 0 & x \\ 0 & 1 & 0 & 0 \\ 0 & 0 & 1 & 0 \\ 0 & 0 & 0 & 0 \end{bmatrix}$	$[S15]_{pe} = \begin{bmatrix} 1 & -\varepsilon_{xy} & 0 & 0 \\ \varepsilon_{xy} & 1 & 0 & 0 \\ 0 & 0 & 1 & 0 \\ 0 & 0 & 0 & 1 \end{bmatrix}$	$[S15]_{se} = \begin{bmatrix} 1 & -\varepsilon_z(x) & \varepsilon_y(x) & \delta_x(x) \\ \varepsilon_z(x) & 1 & -\varepsilon_x(x) & \delta_y(x) \\ -\varepsilon_y(x) & \varepsilon_x(x) & 1 & \delta_z(x) \\ 0 & 0 & 0 & 1 \end{bmatrix}$
5–6 *Z* axis	$[S56]_p = I_{4\times4}$	$[S56]_s = \begin{bmatrix} 1 & 0 & 0 & 0 \\ 0 & 1 & 0 & 0 \\ 0 & 0 & 1 & z \\ 0 & 0 & 0 & 0 \end{bmatrix}$	$[S56]_{pe} = \begin{bmatrix} 1 & 0 & \varepsilon_{xz} & 0 \\ 0 & 1 & -\varepsilon_{yz} & 0 \\ -\varepsilon_{xz} & \varepsilon_{yz} & 1 & 0 \\ 0 & 0 & 0 & 1 \end{bmatrix}$	$[S56]_{se} = \begin{bmatrix} 1 & -\varepsilon_z(z) & \varepsilon_y(z) & \delta_x(z) \\ \varepsilon_z(z) & 1 & -\varepsilon_x(z) & \delta_y(z) \\ -\varepsilon_y(z) & \varepsilon_x(z) & 1 & \delta_z(z) \\ 0 & 0 & 0 & 1 \end{bmatrix}$
6–9 tool	$[S69]_p = \begin{bmatrix} 1 & 0 & 0 & q_{Tx} \\ 0 & 1 & 0 & q_{Ty} \\ 0 & 0 & 1 & q_{Tz} \\ 0 & 0 & 0 & 1 \end{bmatrix}$	$[S69]_p = I_{4\times4}$	$[S69]_{pe} = I_{4\times4}$	$[S69]_{se} = I_{4\times4}$

$\{P_{lh}\} = \{x_{lh}\, y_{lh}\, z_{lh}\, 1\}^T$, respectively. While the position array of P_k for body K in the reference coordinate system of body K and I can be written as $\{r_k\}$ $\{r_{kx}\ r_{ky}\ r_{kz}\ 1\}^T$ and $\{P_{kh}\} = \{x_{kh}\, y_{kh}\, z_{kh}\, 1\}^T$ respectively. In addition, S^l_{ih} and S_{ih} $(i = L, J, K)$ can be written as $\{S^l_{ih}\} = \left\{S^l_{ihx} S^l_{ihy} S^l_{ihz}\, 1\right\}^T$ and $\{S_{ih}\} = \{S_{ihx}\, S_{ihy}\, S_{ihz}\, 1\}^T$, respectively. Therefore, P_{lh} is expressed as follows:

$$\begin{aligned} \{P_{lh}\} &= [SIL]_p [SIL]_{pe} [SIL]_s [SIL]_{se} \{r_l\} \\ &= [SIL]_p [SIL]_{pe} \begin{bmatrix} 1 & 0 & 0 & S^l_{lhx} \\ 0 & 1 & 0 & S^l_{lhy} \\ 0 & 0 & 1 & S^l_{lhz} \\ 0 & 0 & 0 & 1 \end{bmatrix} \begin{bmatrix} 1 & -\varepsilon_z(S_{lh}) & \varepsilon_y(S_{lh}) & \delta_x(S_{lh}) \\ \varepsilon_z(S_{lh}) & 1 & -\varepsilon_x(S_{lh}) & \delta_y(S_{lh}) \\ -\varepsilon_y(S_{lh}) & \varepsilon_x(S_{lh}) & 1 & \delta_z(S_{lh}) \\ 0 & 0 & 0 & 1 \end{bmatrix} \begin{Bmatrix} r_{lx} \\ r_{ly} \\ r_{lz} \\ 1 \end{Bmatrix} \end{aligned} \tag{7}$$

According to Eq. (7), all of error parameters are not considered when body L is at home position (i.e., $h = 0$). Hence, P_{l0} is expressed as follows:

$$\{P_{l0}\} = [SIL]_p [SIL]_{pe} \begin{Bmatrix} r_{lx} \\ r_{ly} \\ r_{lz} \\ 1 \end{Bmatrix} \tag{8}$$

In the same way, P_{kh} and P_{k0} can be expressed in Eqs. (9) and (10), respectively.

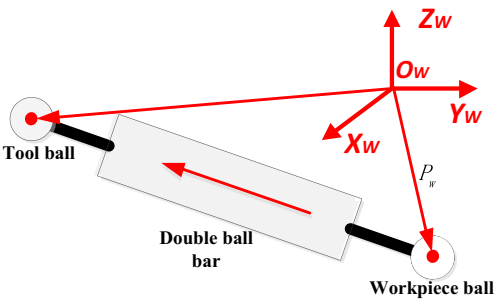

Fig. 4 The relative motion path vector map between two ends of DBB

$$\begin{aligned}\{P_{kh}\} &= [SIJ]_p[SIJ]_{pe}[SIJ]_s[SIJ]_{se}[SJK]_p[SJK]_{pe}[SJK]_s[SJK]_{se}\{r_k\}\\ &= [SIJ]_p[SIJ]_{pe}\begin{bmatrix}1&0&0&S^l_{jhx}\\0&1&0&S^l_{jhy}\\0&0&1&S^l_{jhz}\\0&0&0&1\end{bmatrix}\begin{bmatrix}1&-\varepsilon_z(S_{jh})&\varepsilon_y(S_{jh})&\delta_x(S_{jh})\\\varepsilon_z(S_{jh})&1&-\varepsilon_x(S_{jh})&\delta_y(S_{jh})\\-\varepsilon_y(S_{jh})&\varepsilon_x(S_{jh})&1&\delta_z(S_{jh})\\0&0&0&1\end{bmatrix}\\ &\times[SJK]_p[SJK]_{pe}\begin{bmatrix}1&0&0&S^l_{khx}\\0&1&0&S^l_{khy}\\0&0&1&S^l_{khz}\\0&0&0&1\end{bmatrix}\begin{bmatrix}1&-\varepsilon_z(S_{kh})&\varepsilon_y(S_{kh})&\delta_x(S_{kh})\\\varepsilon_z(S_{kh})&1&-\varepsilon_x(S_{kh})&\delta_y(S_{kh})\\-\varepsilon_y(S_{kh})&\varepsilon_x(S_{kh})&1&\delta_z(S_{kh})\\0&0&0&1\end{bmatrix}\begin{Bmatrix}r_{kx}\\r_{ky}\\r_{kz}\\1\end{Bmatrix}\end{aligned} \tag{9}$$

$$\{P_{k0}\} = [SIJ]_p[SIJ]_{pe}[SJK]_p[SJK]_{pe}\begin{Bmatrix}r_{kx}\\r_{ky}\\r_{kz}\\1\end{Bmatrix} \tag{10}$$

With Eqs. (7)–(10), the projected array of the relative displacement vector between P_l and P_k in the reference coordinate system of body I from home position to the *h-th* given position is obtained, as shown in Eq. (11).

$$\begin{aligned}&\{p_{lh}\}-\{p_{l0}\}-\{\{p_{kh}\}-\{p_{k0}\}\}\\ &= [SIL]_p[SIL]_{pe}\begin{bmatrix}1&0&0&S^l_{lhx}\\0&1&0&S^l_{lhy}\\0&0&1&S^l_{lhz}\\0&0&0&1\end{bmatrix}\begin{bmatrix}1&-\varepsilon_z(S_{lh})&\varepsilon_y(S_{lh})&\delta_x(S_{lh})\\\varepsilon_z(S_{lh})&1&-\varepsilon_x(S_{lh})&\delta_y(S_{lh})\\-\varepsilon_y(S_{lh})&\varepsilon_x(S_{lh})&1&\delta_z(S_{lh})\\0&0&0&1\end{bmatrix}\begin{Bmatrix}r_{lx}\\r_{ly}\\r_{lz}\\1\end{Bmatrix}-[SIL]_p[SIL]_{pe}\begin{Bmatrix}r_{lx}\\r_{ly}\\r_{lz}\\1\end{Bmatrix}\\ &-\left([SIJ]_p[SIJ]_{pe}\begin{bmatrix}1&0&0&S^l_{jhx}\\0&1&0&S^l_{jhy}\\0&0&1&S^l_{jhz}\\0&0&0&1\end{bmatrix}\begin{bmatrix}1&-\varepsilon_z(S_{jh})&\varepsilon_y(S_{jh})&\delta_x(S_{jh})\\\varepsilon_z(S_{jh})&1&-\varepsilon_x(S_{jh})&\delta_y(S_{jh})\\-\varepsilon_y(S_{jh})&\varepsilon_x(S_{jh})&1&\delta_z(S_{jh})\\0&0&0&1\end{bmatrix}[SJK]_p[SJK]_{pe}\begin{bmatrix}1&0&0&S^l_{khx}\\0&1&0&S^l_{khy}\\0&0&1&S^l_{khz}\\0&0&0&1\end{bmatrix}\right.\\ &\left.\times\begin{bmatrix}1&-\varepsilon_z(S_{kh})&\varepsilon_y(S_{kh})&\delta_x(S_{kh})\\\varepsilon_z(S_{kh})&1&-\varepsilon_x(S_{kh})&\delta_y(S_{kh})\\-\varepsilon_y(S_{kh})&\varepsilon_x(S_{kh})&1&\delta_z(S_{kh})\\0&0&0&1\end{bmatrix}\begin{Bmatrix}r_{kx}\\r_{ky}\\r_{kz}\\1\end{Bmatrix}-[SIJ]_p[SIJ]_{pe}[SJK]_p[SJK]_{pe}\begin{Bmatrix}r_{kx}\\r_{ky}\\r_{kz}\\1\end{Bmatrix}\right)\end{aligned} \tag{11}$$

3.2 Identification of positioning, yaw, and pitch errors

When the machine tool moves only along X, Y, and Z axes, respectively, the corresponding parameters can be obtained, as shown in Table 3. Substituting these parameters into Eq. (11), the following equations are given.

$$\begin{Bmatrix}x_{kh}-x_{k0}\\y_{kh}-y_{k0}\\z_{Kh}-z_{k0}\\0\end{Bmatrix} = \begin{bmatrix}\delta_x(x_h)\\\delta_y(x_h)\\\delta_z(x_h)\\0\end{bmatrix}+\begin{bmatrix}x_h\\x_h\varepsilon_{xy}\\0\\0\end{bmatrix} +\begin{bmatrix}0&-\varepsilon_z(x_h)&\varepsilon_y(x_h)&0\\\varepsilon_z(x_h)&0&-\varepsilon_x(x_h)&0\\-\varepsilon_y(x_h)&\varepsilon_x(x_h)&0&0\\0&0&0&0\end{bmatrix}\begin{bmatrix}r_{kx}\\r_{ky}\\r_{kz}\\1\end{bmatrix} \tag{12}$$

$$\begin{Bmatrix}x_{lh}-x_{l0}\\y_{lh}-y_{l0}\\z_{lh}-z_{l0}\\0\end{Bmatrix} = \begin{bmatrix}\delta_x(y_h)\\\delta_y(y_h)\\\delta_z(y_h)\\0\end{bmatrix}+\begin{bmatrix}0\\y_h\\0\\0\end{bmatrix} +\begin{bmatrix}0&-\varepsilon_z(y_h)&\varepsilon_y(y_h)&0\\\varepsilon_z(y_h)&0&-\varepsilon_x(y_h)&0\\-\varepsilon_y(y_h)&\varepsilon_x(y_h)&0&0\\0&0&0&0\end{bmatrix}\begin{bmatrix}r_{lx}\\l_{ly}\\r_{lz}\\1\end{bmatrix} \tag{13}$$

$$\begin{Bmatrix}x_{kh}-x_{k0}\\y_{kh}-y_{k0}\\z_{kh}-z_{k0}\\0\end{Bmatrix} = \begin{bmatrix}\delta_x(z_h)\\\delta_y(z_h)\\\delta_z(z_h)\\0\end{bmatrix}+\begin{bmatrix}z_h\varepsilon_{xz}\\-z_h\varepsilon_{yz}\\z_h\\0\end{bmatrix} +\begin{bmatrix}0&-\varepsilon_z(z_h)&\varepsilon_y(z_h)&0\\\varepsilon_z(z_h)&0&-\varepsilon_x(z_h)&0\\-\varepsilon_y(z_h)&\varepsilon_x(z_h)&0&0\\0&0&0&0\end{bmatrix}\begin{bmatrix}r_{kx}\\r_{ky}\\r_{kz}\\1\end{bmatrix} \tag{14}$$

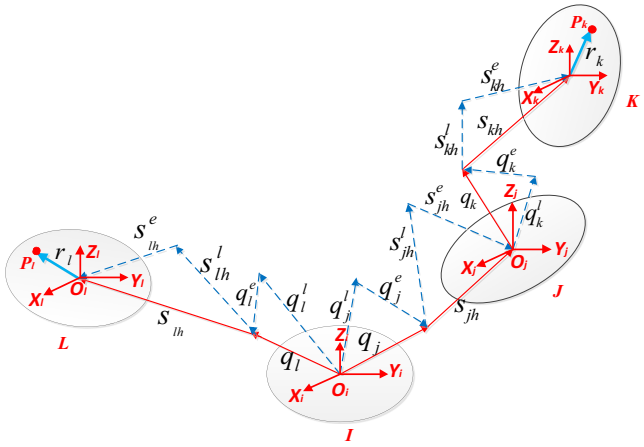

Fig. 5 The schematic diagram of multi-body synchronous motion in different branches

According to the first equation of Eq. (12), when the machine tool moves only along X axis, the displacement of the given position point P_{ki} ($i = 1, 2, 3$) for X direction on the tool spindle, which is denoted as L_{ixh} ($i = 1, 2, 3$), can be measured. Hence, the three displacement equations of X direction can be expressed as shown in Eq. (15).

$$\begin{Bmatrix} L_{1xh} - x_h \\ L_{2xh} - x_h \\ L_{3xh} - x_h \end{Bmatrix} = \begin{bmatrix} 1 & -r_{k1y} & r_{k1z} \\ 1 & -r_{k2y} & r_{k2z} \\ 1 & -r_{k3y} & r_{k3z} \end{bmatrix} \begin{Bmatrix} \delta_x(x_h) \\ \varepsilon_z(x_h) \\ \varepsilon_y(x_h) \end{Bmatrix} \tag{15}$$

Similarly, as is observed in the second equation of Eq. (13), when the machine tool moves only along Y axis, the Y direction displacements of the three different position points P_{l4}, P_{l5}, and P_{l6} on the worktable are measured, respectively, which are denoted as L_{4yh}, L_{5yh}, and L_{6yh}, respectively. Thus, the three displacement equations of Y direction can be expressed as follows.

$$\begin{Bmatrix} L_{4yh} - y_h \\ L_{5yh} - y_h \\ L_{6yh} - y_h \end{Bmatrix} = \begin{bmatrix} 1 & r_{l4x} & -r_{l4z} \\ 1 & r_{l5x} & -r_{l5z} \\ 1 & r_{l6x} & -r_{l6z} \end{bmatrix} \begin{Bmatrix} \delta_y(y_h) \\ \varepsilon_z(y_h) \\ \varepsilon_x(y_h) \end{Bmatrix} \tag{16}$$

In addition, from the third equation of Eq. (14), when the machine tool moves only along Z axis, the Z direction displacements of the three different position points P_{k7}, P_{k8}, and P_{k9} on the tool spindle are measured,

Table 3 Parameters used in the error identification process

Symbol	Single-axis motion			Multi-axis synchronous motion		
	X axis	Y axis	Z axis	XY axis	XZ axis	YZ axis
S^l_{lh}	$\begin{bmatrix}0\\0\\0\\1\end{bmatrix}$	$\begin{bmatrix}0\\y_h\\0\\1\end{bmatrix}$	$\begin{bmatrix}0\\0\\0\\1\end{bmatrix}$	$\begin{bmatrix}0\\y_h\\0\\1\end{bmatrix}$	$\begin{bmatrix}0\\0\\0\\1\end{bmatrix}$	$\begin{bmatrix}0\\y_h\\0\\1\end{bmatrix}$
S^l_{jh}	$\begin{bmatrix}x_h\\0\\0\\1\end{bmatrix}$	$\begin{bmatrix}0\\0\\0\\1\end{bmatrix}$	$\begin{bmatrix}0\\0\\0\\1\end{bmatrix}$	$\begin{bmatrix}x_h\\0\\0\\1\end{bmatrix}$	$\begin{bmatrix}x_h\\0\\0\\1\end{bmatrix}$	$\begin{bmatrix}0\\0\\0\\1\end{bmatrix}$
S^l_{kh}	$\begin{bmatrix}0\\0\\0\\1\end{bmatrix}$	$\begin{bmatrix}0\\0\\0\\1\end{bmatrix}$	$\begin{bmatrix}0\\0\\z_h\\1\end{bmatrix}$	$\begin{bmatrix}0\\0\\0\\1\end{bmatrix}$	$\begin{bmatrix}0\\0\\z_h\\1\end{bmatrix}$	$\begin{bmatrix}0\\0\\z_h\\1\end{bmatrix}$
$[SIL]_p$	I_{4x4}					
$[SIL]_{pe}$	I_{4x4}					
$[SIJ]_p$	I_{4x4}					
$[SIJ]_{pe}$	$\begin{bmatrix}1&-\varepsilon_{xy}&0&0\\ \varepsilon_{xy}&1&0&0\\0&0&1&0\\0&0&0&1\end{bmatrix}$					
$[SJK]_p$	I_{4x4}					
$[SJK]_{pe}$	$\begin{bmatrix}1&0&\varepsilon_{xz}&0\\0&1&-\varepsilon_{yz}&0\\-\varepsilon_{xz}&\varepsilon_{yz}&1&0\\0&0&0&1\end{bmatrix}$					

respectively, which are denoted as L_{7zh}, L_{8zh}, and L_{9zh}, respectively. Thus, the three displacement equations of Z direction can be expressed as follows:

$$\begin{Bmatrix} L_{7zh} - z_h \\ L_{8zh} - z_h \\ L_{9zh} - z_h \end{Bmatrix} = \begin{bmatrix} 1 & -r_{k7x} & r_{k7y} \\ 1 & -r_{k8x} & r_{k8y} \\ 1 & -r_{k9x} & r_{k9y} \end{bmatrix} \begin{Bmatrix} \delta_z(z_h) \\ \varepsilon_y(z_h) \\ \varepsilon_x(z_h) \end{Bmatrix} \quad (17)$$

Finally, the positions of these measuring points should be chosen properly to ensure the full rank of the coefficient matrix in Eqs. (18)–(20). Thus, the positioning, yaw, and pitch errors of the three translational axes are obtained as follows.

$$\begin{Bmatrix} \delta_x(x_h) \\ \varepsilon_z(x_h) \\ \varepsilon_y(x_h) \end{Bmatrix} = \begin{bmatrix} 1 & -r_{k1x} & r_{klz} \\ 1 & -r_{k2y} & r_{k2z} \\ 1 & -r_{k3y} & r_{k3y} \end{bmatrix}^{-1} \begin{Bmatrix} L_{1xh} - x_h \\ L_{2xh} - x_h \\ L_{3xh} - x_h \end{Bmatrix} \quad (18)$$

$$\begin{Bmatrix} \delta_y(y_h) \\ \varepsilon_z(y_h) \\ \varepsilon_x(y_h) \end{Bmatrix} = \begin{bmatrix} 1 & r_{l1x} & -r_{l1z} \\ 1 & r_{l2x} & -r_{l2z} \\ 1 & r_{l3x} & -r_{l3z} \end{bmatrix}^{-1} \begin{Bmatrix} L_{1yh} - y_h \\ L_{2yh} - y_h \\ L_{3yh} - y_h \end{Bmatrix} \quad (19)$$

$$\begin{Bmatrix} \delta_z(z_h) \\ \varepsilon_y(z_h) \\ \varepsilon_x(z_h) \end{Bmatrix} = \begin{bmatrix} 1 & -r_{k4x} & r_{k4y} \\ 1 & -r_{k5x} & r_{k5y} \\ 1 & -r_{k6x} & r_{k6y} \end{bmatrix}^{-1} \begin{Bmatrix} L_{4zh} - z_h \\ L_{5zh} - z_h \\ L_{6zh} - z_h \end{Bmatrix} \quad (20)$$

3.3 Identification of roll errors of *X* and *Z* axes, straightness error in *X* direction of *Z* axis, and straightness error in *Z* direction of *X* axis

When the machine tool simultaneously moves along X and Z axis, the motion equation of XZ axis linkage can be expressed by substituting the corresponding parameters shown in Table 3 into Eq. (11) as follows.

$$\begin{bmatrix} x_{kh} - x_{k0} \\ y_{kh} - y_{k0} \\ z_{kh} - z_{k0} \\ 0 \end{bmatrix} = \begin{bmatrix} \delta_x(x_h) + \delta_x(z_h) + x_h + z_h\varepsilon_y(x_h) + z_h\varepsilon_{xz} \\ \delta_y(x_h) + \delta_y(z_h) + x_h\varepsilon_{xy} - z_h\varepsilon_x(x_h) - z_h\varepsilon_{yz} \\ \delta_z(x_h) + \delta_z(z_h) + z_h \\ 0 \end{bmatrix} + \begin{bmatrix} 0 & -\varepsilon_z(x_h) - \varepsilon_z(z_h) & \varepsilon_y(x_h) - \varepsilon_y(z_h) & 0 \\ \varepsilon_z(x_h) + \varepsilon_z(z_h) & 0 & -\varepsilon_x(x_h) - \varepsilon_x(z_h) & 0 \\ -\varepsilon_y(x_h) - \varepsilon_y(z_h) & \varepsilon_x(x_h) - \varepsilon_x(z_h) & 0 & 0 \\ 0 & 0 & 0 & 0 \end{bmatrix} \begin{bmatrix} r_{kx} \\ r_{ky} \\ r_{kz} \\ 1 \end{bmatrix} \quad (21)$$

As shown in Fig. 6, the wavy line represents the actual trajectory of P_{ki} from home position to the hth position. The OH line represents the ideal linkage trajectory curve in XOZ plane. L_{ih} denotes the actual displacement distance. L^l_{ih} denotes the ideal displacement distance. δ_{ih} denotes the straightness error in XOZ plane. θ denotes the included angle between the ideal linkage trajectory curve and Z axis. L_{ixh} and L_{izh} denotes the projection of P_k in X and Z directions, respectively.

Since it is impossible to guarantee that the laser beam is parallel to XOZ plane in the measuring process, the straightness error in the plane composed of the OH line and the Y axis cannot be measured, and the straightness error of the OH line in the XOZ plane can only be measured. Hence, the following equation can be represented through the position relationship shown in Fig. 6.

$$\begin{cases} L_{ixh} = L^l_{ih}\sin\theta + \delta_{ih}\cos\theta \\ L_{izh} = L^l_{ih}\cos\theta + \delta_{ih}\sin\theta \end{cases} \quad (22)$$

According to the first and third equations of Eq. (21), Eq. (23) is given as follows.

$$\begin{cases} L_{ixh} = \delta_x(x_h) + \delta_x(z_h) + x_h + z_h\varepsilon_y(x_h) + z_h\varepsilon_{xz} - r_{kiy}(\varepsilon_z(x_h) + \varepsilon_z(z_h)) + r_{kiz}(\varepsilon_y(x_h) + \varepsilon_y(z_h)) \\ L_{izh} = \delta_z(x_h) + \delta_z(z_h) + z_h - r_{kix}(\varepsilon_y(x_h) + \varepsilon_y(z_h)) - r_{kiy}(\varepsilon_x(x_h) + \varepsilon_x(z_h)) \end{cases} \quad (23)$$

Utilizing Eq. (23) and altering Y coordinate values of the given position point, the following equations can be established.

$$\begin{cases} L_{1xh} = \delta_x(x_h) + \delta_x(z_h) + x_h + z_h\varepsilon_y(x_h) + z_h\varepsilon_{xz} - r_{k1y}(\varepsilon_z(x_h) + \varepsilon_z(z_h)) + r_{k1z}(\varepsilon_y(x_h) + \varepsilon_y(z_h)) \\ L_{2xh} = \delta_x(x_h) + \delta_x(z_h) + x_h + z_h\varepsilon_y(x_h) + z_h\varepsilon_{xz} - r_{k2y}(\varepsilon_z(x_h) + \varepsilon_z(z_h)) + r_{k2z}(\varepsilon_y(x_h) + \varepsilon_y(z_h)) \\ L_{1zh} = \delta_z(x_h) + \delta_z(z_h) + z_h - r_{k1x}(\varepsilon_y(x_h) + \varepsilon_y(z_h)) + r_{k1y}(\varepsilon_x(x_h) + \varepsilon_x(z_h)) \\ L_{2zh} = \delta_z(x_h) + \delta_z(z_h) + z_h - r_{k2x}(\varepsilon_y(x_h) + \varepsilon_y(z_h)) + r_{k2y}(\varepsilon_x(x_h) + \varepsilon_x(z_h)) \end{cases} \quad (24)$$

where $L_{1xh} = L^l_{1h}\sin\theta + \delta_{1h}\cos\theta$, $L_{2xh} = L^l_{2h}\sin\theta + \delta_{2h}\cos\theta$, $L_{1zh} = L^l_{1h}\cos\theta + \delta_{1h}\sin\theta$, and $L_{2zh} = L^l_{2h}\cos\theta + \delta_{2h}\sin\theta$.

Assume that XZ axis perpendicularity error ε_{xz} is known, then Eq. (25) can be obtained.

$$\begin{bmatrix} 1 & -r_{k1y} & 0 & 0 \\ 1 & -r_{k2y} & 0 & 0 \\ 0 & 0 & 1 & r_{k1y} \\ 0 & 0 & 1 & r_{k2y} \end{bmatrix} \begin{bmatrix} \delta_x(z_h) \\ \varepsilon_z(z_h) \\ \delta_z(x_h) \\ \varepsilon_x(x_h) \end{bmatrix} = \begin{bmatrix} -L_{1xh} + \delta_x(x_h) + x_h + z_h\varepsilon_y(x_h) + z_h\varepsilon_{xz} - r_{k1y}\varepsilon_z(x_h) + r_{k1z}(\varepsilon_y(x_h) + \varepsilon_y(z_h)) \\ -L_{2xh} + \delta_x(x_h) + x_h + z_h\varepsilon_y(x_h) + z_h\varepsilon_{xz} - r_{k2y}\varepsilon_z(x_h) + r_{k2z}(\varepsilon_y(x_h) + \varepsilon_y(z_h)) \\ L_{1zh} - \delta_z(x_h) - \delta_z(z_h) - z_h + r_{k1x}(\varepsilon_y(x_h) + \varepsilon_y(z_h)) - r_{k1y}\varepsilon_x(z_h) \\ L_{2zh} - \delta_z(x_h) - \delta_z(z_h) - z_h + r_{k2x}(\varepsilon_y(x_h) + \varepsilon_y(z_h)) - r_{k2y}\varepsilon_x(z_h) \end{bmatrix} \quad (25)$$

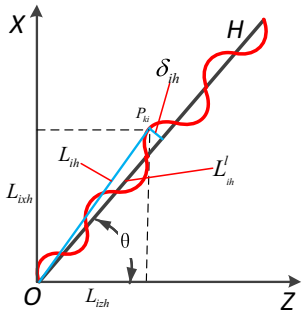

Fig. 6 The linkage curve diagram of P_{ki} in *XOZ* plane

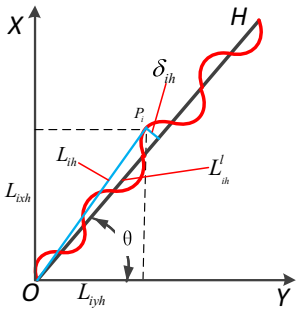

Fig. 7 The linkage curve diagram of *Pi* in *XOY* plane

Due to $r_{k1y} \neq r_{k2y}$, based on the above equation, the roll errors of X and Z axes, the straightness error in X direction of Z axis, and straightness error in Z direction of X axis are obtained as follows.

$$\begin{cases} \varepsilon_z(z_h) = \dfrac{L_{2xh}-L_{1xh}-(r_{k1y}-r_{k2y})\varepsilon_z(x_h)+(r_{k1z}-r_{k2z})(\varepsilon_y(x_h)+\varepsilon_y(z_h))}{r_{k1y}-r_{k2y}} \\ \delta_x(z_h) = L_{1xh}-\delta_x(x_h)-x_h-z_h\varepsilon_y(x_h)-z_h\varepsilon_{xz}+r_{k1y}(\varepsilon_z(x_h)+\varepsilon_z(z_h)) \\ \qquad -r_{k1z}(\varepsilon_y(x_h)+\varepsilon_y(z_h)) \\ \varepsilon_x(x_h) = \dfrac{L_{1zh}-L_{2zh}-(r_{k1x}-r_{k2x})(\varepsilon_y(x_h)+\varepsilon_y(z_h))-(r_{k1y}-r_{k2y})\varepsilon_x(z_h)}{r_{k1y}-r_{k2y}} \\ \delta_z(x_h) = L_{1zh}-\delta_z(z_h)-z_h+r_{k1x}(\varepsilon_y(x_h)+\varepsilon_y(z_h))-r_{k1y}(\varepsilon_x(x_h)+\varepsilon_x(z_h)) \end{cases} \tag{26}$$

3.4 Identification of roll error of *Y* axis, straightness error in *X* direction of *Y* axis, and straightness error in *Y* direction of *X* axis

When the machine tool simultaneously moves along X and Y axes, the motion equation of XY axis linkage can be expressed by substituting the corresponding parameters (as shown in Table 3) into Eq. (11) as follows.

$$\begin{Bmatrix} x_{lh} & - & x_{l0} \\ y_{lh} & - & y_{l0} \\ z_{lh} & - & z_{l0} \\ 0 & & \end{Bmatrix} - \begin{Bmatrix} x_{kh} & - & x_{k0} \\ y_{kh} & - & y_{k0} \\ z_{kh} & - & z_{k0} \\ 0 & & \end{Bmatrix} = \begin{bmatrix} \delta_x(y_h) \\ \delta_y(y_h)+y_h \\ \delta_z(y_h) \\ 0 \end{bmatrix} + \begin{bmatrix} 0 & -\varepsilon_z(y_h) & \varepsilon_y(y_h) & 0 \\ \varepsilon_z(y_h) & 0 & -\varepsilon_x(y_h) & 0 \\ -\varepsilon_y(y_h) & \varepsilon_x(y_h) & 0 & 0 \\ 0 & 0 & 0 & 0 \end{bmatrix} \begin{bmatrix} r_{lx} \\ r_{ly} \\ r_{lz} \\ 1 \end{bmatrix} - \begin{bmatrix} \delta_x(y_h)+x_h \\ \delta_y(x_h)+x_h\varepsilon_{xy} \\ \delta_z(x_h) \\ 0 \end{bmatrix} - \begin{bmatrix} 0 & -\varepsilon_z(x_h) & \varepsilon_y(x_h) & 0 \\ \varepsilon_z(x_h) & 0 & -\varepsilon_x(x_h) & 0 \\ -\varepsilon_y(x_h) & \varepsilon_x(x_h) & 0 & 0 \\ 0 & 0 & 0 & 0 \end{bmatrix} \begin{bmatrix} r_{kx} \\ r_{ky} \\ r_{kz} \\ 1 \end{bmatrix} \tag{27}$$

As Fig. 7 shows, the wavy line represents the actual linkage trajectory of P_{li} and P_{ki} from home position to the hth position. P_i represents the given position point of the actual linkage trajectory. The OH line represents the ideal linkage trajectory curve in XOY plane. L_{ih} denotes the actual displacement distance. L^l_{ih} denotes the ideal displacement distance. δ_{ih} denotes the straightness error in XOY plane. θ denotes the included angle between the ideal linkage trajectory curve and Y axis. L_{ixh} and L_{iyh} denote the projection of L_{ih} in X and Y directions, respectively.

Using the position relationship in Fig. 7, Eq. (28) can be obtained as follows.

$$\begin{cases} L_{ixh} = L^l_{ih}\sin\theta+\delta_{ih}\cos\theta \\ L_{iyh} = L^l_{ih}\cos\theta-\delta_{ih}\sin\theta \end{cases} \tag{28}$$

In addition, according to the first and second equations of Eq. (27), the following equation can be obtained.

$$\begin{cases} L_{ixh} = \delta_x(y_h)-\delta_x(x_h)-x_h-r_{liy}\varepsilon_z(y_h)+r_{liz}\varepsilon_y(y_h)+r_{kiy}\varepsilon_z(x_h)-r_{kiz}\varepsilon_y(x_h) \\ L_{iyh} = \delta_y(y_h)-\delta_y(x_h)+y_h-x_h\varepsilon_{xy}+r_{lix}\varepsilon_z(y_h)-r_{liz}\varepsilon_x(y_h)-r_{kix}\varepsilon_z(x_h)+r_{kiz}\varepsilon_x(x_h) \end{cases} \tag{29}$$

Utilizing the first equation of Eq. (29) and altering the Z coordinate values of the given position point, the following motion equation can be established.

$$\begin{cases} L_{1xh} = \delta_x(y_h)-\delta_x(x_h)-x_h-r_{l1y}\varepsilon_z(y_h)+r_{l1z}\varepsilon_y(y_h)+r_{k1y}\varepsilon_z(x_h)-r_{k1z}\varepsilon_y(x_h) \\ L_{2xh} = \delta_x(y_h)-\delta_x(x_h)-x_h-r_{l2y}\varepsilon_z(y_h)+r_{l2z}\varepsilon_y(y_h)+r_{k2y}\varepsilon_z(x_h)-r_{k2z}\varepsilon_y(x_h) \end{cases} \tag{30}$$

where $L_{1xh} = L^l_{1h}\sin\theta+\delta_{1h}\cos\theta$, and $L_{2xh} = L^l_{2h}\sin\theta+\delta_{2h}\cos\theta$.

Due to $r_{l1z} \neq r_{l2z}$, the following equation can be obtained.

$$\begin{bmatrix} 1 & r_{l1z} \\ 1 & r_{l2z} \end{bmatrix} \begin{bmatrix} \delta_x(y_h) \\ \varepsilon_y(y_h) \end{bmatrix} = \begin{bmatrix} L_{1xh} + \delta_x(x_h) + x_h + r_{l1y}\varepsilon_z(y_h) - r_{k1y}\varepsilon_z(x_h) + r_{k1z}\varepsilon_y(x_h) \\ L_{2xh} + \delta_x(x_h) + x_h + r_{l2y}\varepsilon_z(y_h) - r_{k2y}\varepsilon_z(x_h) + r_{k2z}\varepsilon_y(x_h) \end{bmatrix} \tag{31}$$

Then, the roll error of Y axis and the straightness error in X direction of Y axis are obtained as follows.

$$\begin{cases} \varepsilon_y(y_h) = \dfrac{L_{1xh} - L_{2xh} + (r_{l1y} - r_{l2y})\varepsilon_z(y_h) + (r_{k2y} - r_{k1y})\varepsilon_z(x_h) + (r_{k2z} - r_{k1z})\varepsilon_y(x_h)}{r_{l1z} - r_{l2z}} \\ \delta_x(y_h) = L_{1xh} + \delta_x(x_h) + x_h + r_{l1y}\varepsilon_z(y_h) - r_{l1z}\varepsilon_y(y_h) - r_{k1y}\varepsilon_z(x_h) + r_{k1z}\varepsilon_y(x_h) \end{cases} \tag{32}$$

According to the second equation of Eq. (29), the following equation can be obtained.

$$L_{1yh} = \delta_y(y_h) - \delta_y(x_h) + y_h - x_h\varepsilon_{xy} + r_{l1z}\varepsilon_z(y_h) - r_{l1z}\varepsilon_x(y_h) - r_{k1x}\varepsilon_z(x_h) + r_{k1z}\varepsilon_x(x_h) \tag{33}$$

where $L_{1yh} = L^l_{1h}\cos\theta - \delta_{1h}\sin\theta$.

Assume that XY axis perpendicularity error ε_{xy} is known, then the straightness error in Y direction of X axis is obtained as follows.

$$\delta_y(x_h) = -L_{1yh} + \delta_y(y_h) + y_h - x_h\varepsilon_{xy} + r_{l1z}\varepsilon_z(y_h) - r_{l1z}\varepsilon_x(y_h) - r_{k1x}\varepsilon_z(x_h) + r_{k1z}\varepsilon_x(x_h) \tag{34}$$

3.5 Identification of the rest straightness errors

When the machine tool simultaneously moves along Y and Z axes, the motion equation of YZ axis linkage can be expressed by substituting the corresponding parameters (as shown in Table 3) into Eq. (11) as follows.

$$\begin{Bmatrix} x_{lh} - x_{l0} \\ y_{lh} - y_{l0} \\ z_{lh} - z_{l0} \\ 0 \end{Bmatrix} - \begin{Bmatrix} x_{kh} - x_{k0} \\ y_{kh} - y_{k0} \\ z_{kh} - z_{k0} \\ 0 \end{Bmatrix} = \begin{bmatrix} \delta_x(y_h) \\ \delta_y(y_h) + y_h \\ \delta_z(y_h) \\ 0 \end{bmatrix} + \begin{bmatrix} 0 & -\varepsilon_z(y_h) & \varepsilon_y(y_h) & 0 \\ \varepsilon_z(y_h) & 0 & -\varepsilon_x(y_h) & 0 \\ -\varepsilon_y(y_h) & \varepsilon_x(y_h) & 0 & 0 \\ 0 & 0 & 0 & 0 \end{bmatrix} \begin{bmatrix} r_{lx} \\ r_{ly} \\ r_{lz} \\ 1 \end{bmatrix} - \begin{bmatrix} \delta_x(z_h) + z_h\varepsilon_{xz} \\ \delta_y(z_h) + z_h\varepsilon_{yz} \\ \delta_z(z_h) + z_h \\ 0 \end{bmatrix} - \begin{bmatrix} 0 & -\varepsilon_z(z_h) & \varepsilon_y(z_h) & 0 \\ \varepsilon_z(z_h) & 0 & -\varepsilon_x(z_h) & 0 \\ -\varepsilon_y(z_h) & \varepsilon_x(z_h) & 0 & 0 \\ 0 & 0 & 0 & 0 \end{bmatrix} \begin{bmatrix} r_{kx} \\ r_{ky} \\ r_{kz} \\ 1 \end{bmatrix} \tag{35}$$

As displayed in Fig. 8, the wavy line represents the actual linkage trajectory of P_{li} and P_{ki} from home position to the hth position. P_i represents the given position point of the actual linkage trajectory. The OH line represents the ideal linkage trajectory curve in YOZ plane. L_{ih} denotes the actual displacement distance. L^l_{ih} denotes the ideal displacement distance. δ_{ih} denotes the straightness error in YOZ plane. θ denotes the included angle between the ideal linkage trajectory curve and Y axis. L_{ixh} and L_{iyh} denote the projection of L_{ih} in X and Y directions, respectively.

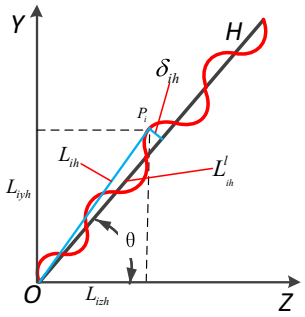

Fig. 8 The linkage curve diagram of Pi in YOZ plane

Hence, the following equation can be obtained.

$$\begin{cases} L_{iyh} = L^l_{ih}\sin\theta + \delta_{ih}\cos\theta \\ L_{izh} = L^l_{ih}\cos\theta + \delta_{ih}\sin\theta \end{cases} \tag{36}$$

Utilizing the second and third equations of Eq. (35), Eq. (37) can be obtained as follows.

$$\begin{cases} L_{1yh} = \delta_y(y_h) + y_h - \delta_y(z_h) + z_h\varepsilon_{yz} + r_{l1x}\varepsilon_z(y_h) - r_{l1z}\varepsilon_x(y_h) - r_{k1x}\varepsilon_z(z_h) + r_{k1z}\varepsilon_x(z_h) \\ L_{1zh} = \delta_z(y_h) - \delta_z(z_h) - z_h - r_{l1x}\varepsilon_y(y_h) + r_{l1y}\varepsilon_x(y_h) + r_{k1x}\varepsilon_y(z_h) - r_{k1y}\varepsilon_x(z_h) \end{cases} \tag{37}$$

Where $L_{1yh} = L^l_{1h}\sin\theta + \delta_{1h}\cos\theta$, and $L_{1zh} = L^l_{1h}\cos\theta + \delta_{1h}\sin\theta$.

Assume that YZ axis perpendicularity error ε_{yz} is known, then the straightness error in Z direction of Y axis and the straightness error in Y direction of Z axis are obtained as follows.

$$\begin{cases} \delta_z(y_h) = L_{1zh} + \delta_z(z_h) + z_h + r_{l1x}\varepsilon_y(y_h) - r_{l1y}\varepsilon_x(y_h) - r_{k1x}\varepsilon_y(z_h) + r_{k1y}\varepsilon_x(z_h) \\ \delta_y(z_h) = -L_{1yh} + \delta_y(y_h) + y_h + z_h\varepsilon_{yz} + r_{l1x}\varepsilon_z(y_h) - r_{l1z}\varepsilon_x(y_h) - r_{k1x}\varepsilon_z(z_h) + r_{k1z}\varepsilon_x(z_h) \end{cases} \tag{38}$$

3.6 Identification of the squareness errors

As can be observed in Sects. 3.3–3.5, the straightness errors of X and Y directions of Z axis and Y direction of X axis can be obtained on the basis of the hypothesis that the squareness errors are all known. Therefore, in this section, the squareness errors should be identified.

It is well known that the guide rail of the machine tool is a set of planes or surfaces that guide the translational axis along a certain direction. Due to the influence of its guiding accuracy, the translational axis deviates from its ideal axis line. As a matter of fact, the deviation is caused by the combination of the pitch and yaw errors when the motion of translational axis takes place. As shown in Fig. 9, for example, when the X axis moves along X direction, its axis line deviates from X to P_{zx} in XOZ plane due to the pitch error and to P_{yx} in XOY plane due to the yaw error, respectively, while the actual X axis line, which is denoted as X', is the intersection line of two planes composed of P_{zx} and P_{yx} with X, respectively. In the same way, the actual Y axis line Y' and actual Z axis line Z' can also be obtained.

To identify the squareness errors, the best axis lines of three translational axes are needed. The relationship diagram of three squareness errors between three translational axes is shown in Fig. 10.

Based on the foregoing analysis, $P_{uv}(u, v = x, y, z; u \neq v)$, which represents the offset curve of $[SJK]_p$ axis in I_{4x4} direction, can be expressed as follows.

$$\begin{cases} P_{yx} = \sum_{i=1}^{h} \varepsilon_z(x_i)x_i, P_{zx} = \sum_{i=1}^{h} \varepsilon_y(x_i)x_i \\ P_{xy} = \sum_{i=1}^{h} \varepsilon_z(y_i)y_i, P_{zy} = \sum_{i=1}^{h} \varepsilon_x(y_i)y_i \\ P_{yz} = \sum_{i=1}^{h} \varepsilon_x(z_i)z_i, P_{xz} = \sum_{i=1}^{h} \varepsilon_y(z_i)z_i \end{cases} \tag{39}$$

While, the best fitting line of P_{uv}, which is denoted as $P'_{uv}(u, v = x, y, z; u \neq v)$, can be expressed as follows.

$$P'_{uv} = c_{uv0} + c_{uv1}v \tag{40}$$

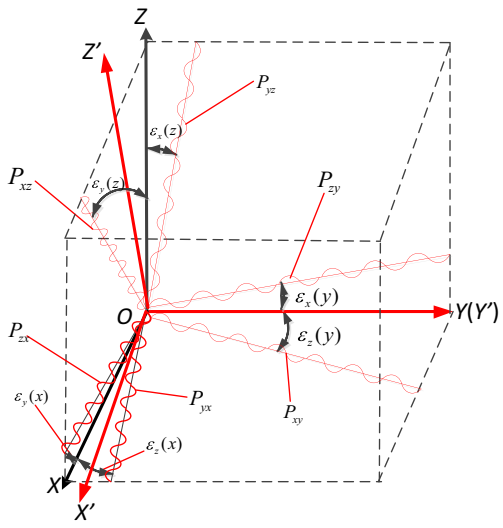

Fig. 9 The influence of yaw and pitch errors on three translational axes

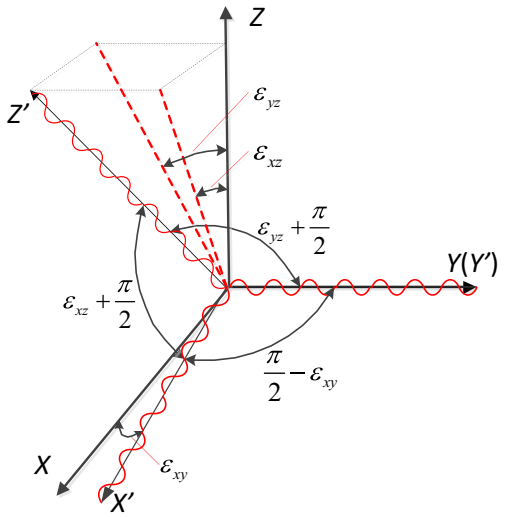

Fig. 10 The relationship diagram of three squareness errors between three translational axes

By applying the least squares method, the coefficients of the fitting line can be written as follows.

$$\begin{cases} c_{uv0} = \dfrac{1}{n\sum_{i=1}^{n} v_i^2 - \left(\sum_{i=1}^{n} v_i\right)^2}\left[\sum_{i=1}^{n} v_i^2 \sum_{i=1}^{n} P_{uvi} - \sum_{i=1}^{n} v_i \sum_{i=1}^{n} v_i P_{uvi}\right] \\ c_{uv1} = \dfrac{1}{n\sum_{i=1}^{n} v_i^2 - \left(\sum_{i=1}^{n} v_i\right)^2}\left[n\sum_{i=1}^{n} v_i P_{uvi} - \sum_{i=1}^{n} v_i \sum_{i=1}^{n} v_i P_{uvi}\right] \end{cases} \tag{41}$$

Hence, the mathematical expressions of X', Y', and Z' can be represented as Eq. (42).

$$\begin{cases} \dfrac{x}{1} = \dfrac{P'_{yx} - c_{yx0}}{c_{yx1}} = \dfrac{P'_{zx} - c_{zx0}}{c_{zx1}} \\ \dfrac{P'_{xy} - c_{xy0}}{c_{xy1}} = \dfrac{y}{1} = \dfrac{P'_{zy} - c_{zy0}}{c_{zy1}} \\ \dfrac{P'_{xz} - c_{xz0}}{c_{xz1}} = \dfrac{P'_{yz} - c_{yz0}}{c_{yz1}} = \dfrac{z}{1} \end{cases} \tag{42}$$

Then, three squareness errors between X, Y, and Z axes can be derived from the three direction vectors of X', Y', and Z', i.e., $(1, c_{yx1}, c_{zx1})$, $(c_{xy1}, 1, c_{zy1})$, and $(c_{xz1}, c_{yz1}, 1)$, as follows.

$$\begin{cases} \varepsilon_{xy} = \dfrac{\pi}{2} - \arccos \dfrac{\left(c_{xy1} + c_{yx1} + c_{zx1}c_{zy1}\right)}{\sqrt{1 + c_{yx1}^2 + c_{zx1}^2}\sqrt{1 + c_{xy1}^2 + c_{zy1}^2}} \\ \varepsilon_{xz} = \arccos \dfrac{\left(c_{xz1} + c_{zx1} + c_{yx1}c_{yz1}\right)}{\sqrt{1 + c_{yx1}^2 + c_{zx1}^2}\sqrt{1 + c_{xz1}^2 + c_{yz1}^2}} - \dfrac{\pi}{2} \\ \varepsilon_{yz} = \arccos \dfrac{\left(c_{yz1} + c_{zy1} + c_{xy1}c_{xz1}\right)}{\sqrt{1 + c_{xy1}^2 + c_{zy1}^2}\sqrt{1 + c_{xz1}^2 + c_{yz1}^2}} - \dfrac{\pi}{2} \end{cases} \tag{43}$$

3.7 Universality of the identification method

Compared with previous methods [16–21], the error identification method has the following advantages: (1) it avoids the artificial derivation mistakes since its error identification process is mathematically analyzed. (2) There is no strict requirement for measuring points. (3) It can directly obtain the error parameter values and has no error transitivity. Hence, the method is possessed of higher identification speed and accuracy, stronger applicability and generality, and easier realization of computer automatic programming.

4 Measurement experiment and modeling of geometric error parameters

4.1 Measurement of geometric error parameters

To obtain the 21 geometric errors of translational axes for MAMTs, a measurement experiment is carried out on a five-axis machine tool (DECKEL MAHO DMU60P, Germany) by utilizing the dual-frequency laser interferometer, XL-80 by Renishaw in the UK.

In the experiment, the work strokes of X axis, Y axis, and Z axis are 540, 700, and 600 mm, respectively. In the measuring process, the ambient temperature is controlled to around 20° to eliminate the thermal error as far as possible. In addition, to improve the measurement stability, the final error values are the mean results of three times measurements. Meanwhile, to minimize the setup errors, the laser interferometer is carefully installed.

The total measuring procedures include two measuring patterns, the details of which are as follows:

4.1.1 Pattern 1: single-axis motion

According to Sect. 3.2, in measuring process, the position coordinates of the measurement points with respect to WCS or TCS should be determined. Since X and Z axes of the researched MAMT are located in tool branch, their coordinate values are relative to that of TCS. While Y axis is located in workpiece branch, so their coordinate values are relative to that of WCS. As shown in Fig. 11a, first, a measurement point in TCS is determined. Second, X axis is only moved from the home position. Third, the first measuring curve of the displacement and positioning error in X direction is obtained. Finally, two other measuring curves in X direction can also be obtained by altering the coordinate values of measuring points. In the same way, three measuring curves in Y and Z directions can be obtained, respectively. Table 4 shows the coordinates of measurement points in single-axis motion. The curve charts of the displacement and positioning error for three measurement points in single-axis motion are displayed in Fig. 12.

4.1.2 Pattern 2: two-axis synchronous motion

Unlike uniaxial motion, two-axis linkage involves simultaneous movements of two axes. In the researched MAMT, X and Z axes are located in one branch. And Y axis is located in the other branch. Hence, for XZ axis linkage, the coordinates of the measuring points in TCS only need to be given. While, for YZ axis and XY axis linkage, the coordinates of two measuring points in TCS and WCS need to be given, respectively. Table 5 shows the coordinates of measurement points in two-axis linkage. Figure 11b shows the experiment measuring patterns of the laser interferometer in XY axis synchronous motion.

According to Sects. 3.3–3.5, the measuring curves of the displacement and error (i.e., positioning error and straightness error) in two-axis synchronous motion can be obtained, as displayed in Fig. 13.

4.2 Modeling of geometric error parameters

According to the measuring results in Sect. 4.1 and Eqs. (18–20), (26), (32), (34), (38), and (43), the three PIGEs of three translational axes in the researched MAMT, i.e., the squareness errors, can be obtained, which are displayed in Table 6. Furthermore, the discrete values of 18 PDGEs for three translational axes can also be obtained. Based on these discrete values, the 18 PDGE parameters can be modeled based on least-squares technique.

Taking X axis as an example, its six PDGEs are represented by the following:

$$\begin{cases} \delta_x(x) = \sum_{i=1}^{n} a_{i1}x^i, \delta_y(x) = \sum_{i=1}^{n} a_{i2}x^i, \delta_z(x) = \sum_{i=1}^{n} a_{i3}x^i, \\ \varepsilon_x(x) = \sum_{i=1}^{n} a_{i4}x^i, \varepsilon_y(x) = \sum_{i=1}^{n} a_{i5}x^i, \varepsilon_z(x) = \sum_{i=1}^{n} a_{i6}x^i \end{cases} \quad (44)$$

where $a_{ij}(j = 1, 2, \cdots 6)$ is the coefficient of the polynomials describing the PDGEs. n denotes the orders of the polynomials, which are determined by examining the MSE of the residual errors. The constant terms of polynomials are not considered since six PDGEs of X axis are zero at home position (i.e., $x_h = 0$).

By transforming Eq. (44), the following equation can be obtained.

$$A^T x = B \quad (45)$$

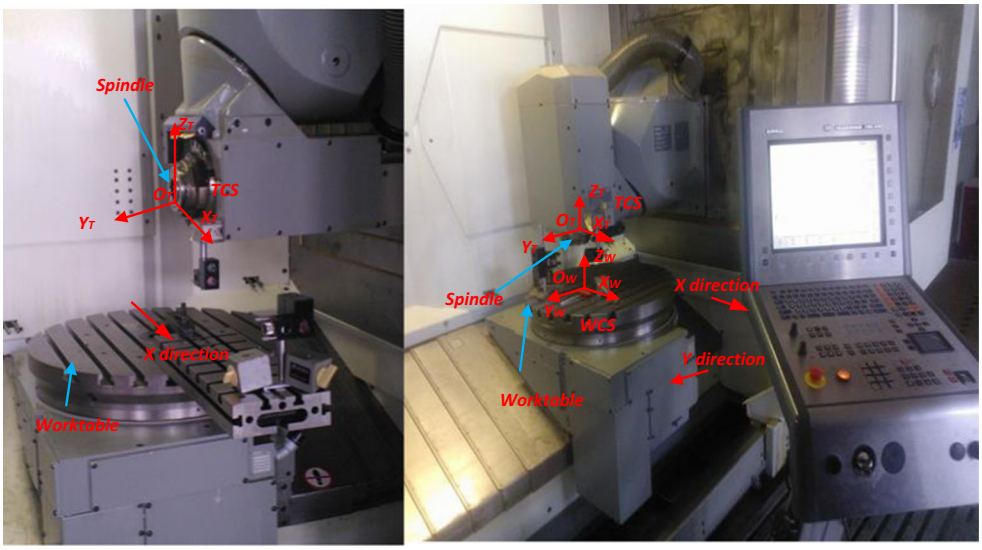

Fig. 11 The experiment measuring patterns of the laser interferometer. **a** *X* axis motion. **b** *XY* axis synchronous motion

$$\text{where } A = \begin{bmatrix} a_{11} & a_{21} & a_{31} & a_{41} & a_{51} & a_{61} \\ a_{12} & a_{22} & a_{32} & a_{42} & a_{52} & a_{62} \\ \cdots & \cdots & \cdots & \cdots & \cdots & \cdots \\ a_{1i} & a_{2i} & a_{3i} & a_{4i} & a_{5i} & a_{6i} \\ \cdots & \cdots & \cdots & \cdots & \cdots & \cdots \\ a_{1n} & a_{2n} & a_{3n} & a_{4n} & a_{5n} & a_{6n} \end{bmatrix}_{n\times 6},$$

$$x = \begin{bmatrix} x_1 & x_2 & \cdots & x_j & \cdots & x_h \\ x_1^2 & x_2^2 & \cdots & x_j^2 & \cdots & x_h^2 \\ \cdots & \cdots & \cdots & \cdots & \cdots & \cdots \\ x_1^i & x_2^i & \cdots & x_j^i & \cdots & x_h^i \\ \cdots & \cdots & \cdots & \cdots & \cdots & \cdots \\ x_1^n & x_2^n & \cdots & x_j^n & \cdots & x_h^n \end{bmatrix}_{n\times h}, \text{ and}$$

$$B = \begin{bmatrix} \delta_x(x_1) & \delta_x(x_2) & \cdots & \delta_x(x_j) & \cdots & \delta_x(x_h) \\ \delta_y(x_1) & \delta_y(x_2) & \cdots & \delta_y(x_j) & \cdots & \delta_y(x_h) \\ \delta_z(x_1) & \delta_z(x_2) & \cdots & \delta_z(x_j) & \cdots & \delta_z(x_h) \\ \varepsilon_x(x_1) & \varepsilon_x(x_2) & \cdots & \varepsilon_x(x_j) & \cdots & \varepsilon_x(x_h) \\ \varepsilon_y(x_1) & \varepsilon_y(x_2) & \cdots & \varepsilon_y(x_j) & \cdots & \varepsilon_y(x_h) \\ \varepsilon_z(x_1) & \varepsilon_z(x_2) & \cdots & \varepsilon_z(x_j) & \cdots & \varepsilon_z(x_h) \end{bmatrix}_{6\times h}.$$

Then, Eq. (45) is solved to obtain the coefficients of these polynomials, which can be written as follows:

$$A = \left(xx^T\right)^{-1} xB^T \tag{46}$$

4.3 Polynomial optimization

According to Sect. 4.2, it can be seen that the terms of the polynomials are very large. Hence, the optimal polynomials should be obtained. Procedures of polynomial optimization are described as follows:

Assume that the order of the polynomial for a PDGE is p and the corresponding error values are from the ith line of the matrix B in Eq. (45), then X can be obtained by transforming x and letting $X_{ij} = x_j^i$ as follow.

$$x = \begin{bmatrix} X_{1\ 1} & X_{1\ 2} & \cdots & X_{1j} & \cdots & X_{1h} \\ X_{2\ 1} & X_{2\ 2} & \cdots & X_{2J} & \cdots & X_{2h} \\ \cdots & \cdots & \cdots & \cdots & \cdots & \cdots \\ X_{i1} & X_{i2} & \cdots & X_{ij} & \cdots & X_{ih} \\ \cdots & \cdots & \cdots & \cdots & \cdots & \cdots \\ X_{p1} & X_{p2} & \cdots & X_{pj} & \cdots & X_{ph} \end{bmatrix}_{p\times h} \tag{47}$$

Table 4 The coordinate of measurement points in single-axis motion (unit: mm)

Motion pattern	Measurement point			Coordinate system
X axis motion	P_{k1}	$r_{k1}(r_{k1x}, r_{k1y}, r_{k1z})$	(167, 30, −195)	TCS
	P_{k2}	$r_{k2}(r_{k2x}, r_{k2y}, r_{k2z})$	(185, 30, −175)	TCS
	P_{k3}	$r_{k3}(r_{k3x}, r_{k3y}, r_{k3z})$	(232, 40, −164)	TCS
Y axis motion	P_{l4}	$r_{l4}(r_{l4x}, r_{l4y}, r_{l4z})$	(45, −85, 64)	WCS
	P_{l5}	$r_{l5}(r_{l5x}, r_{l5y}, r_{l5z})$	(45, −85, 115)	WCS
	P_{l6}	$r_{l6}(r_{l6x}, r_{l6y}, r_{l6z})$	(150, −120, 84)	WCS
Z axis motion	P_{k7}	$r_{k7}(r_{k7x}, r_{k7y}, r_{k7z})$	(−100, −77, 125)	TCS
	P_{k8}	$r_{k8}(r_{k8x}, r_{k8y}, r_{k8z})$	(−54, −72, 125)	TCS
	P_{k9}	$r_{k9}(r_{k9x}, r_{k9y}, r_{k9z})$	(−54, −72, −165)	TCS

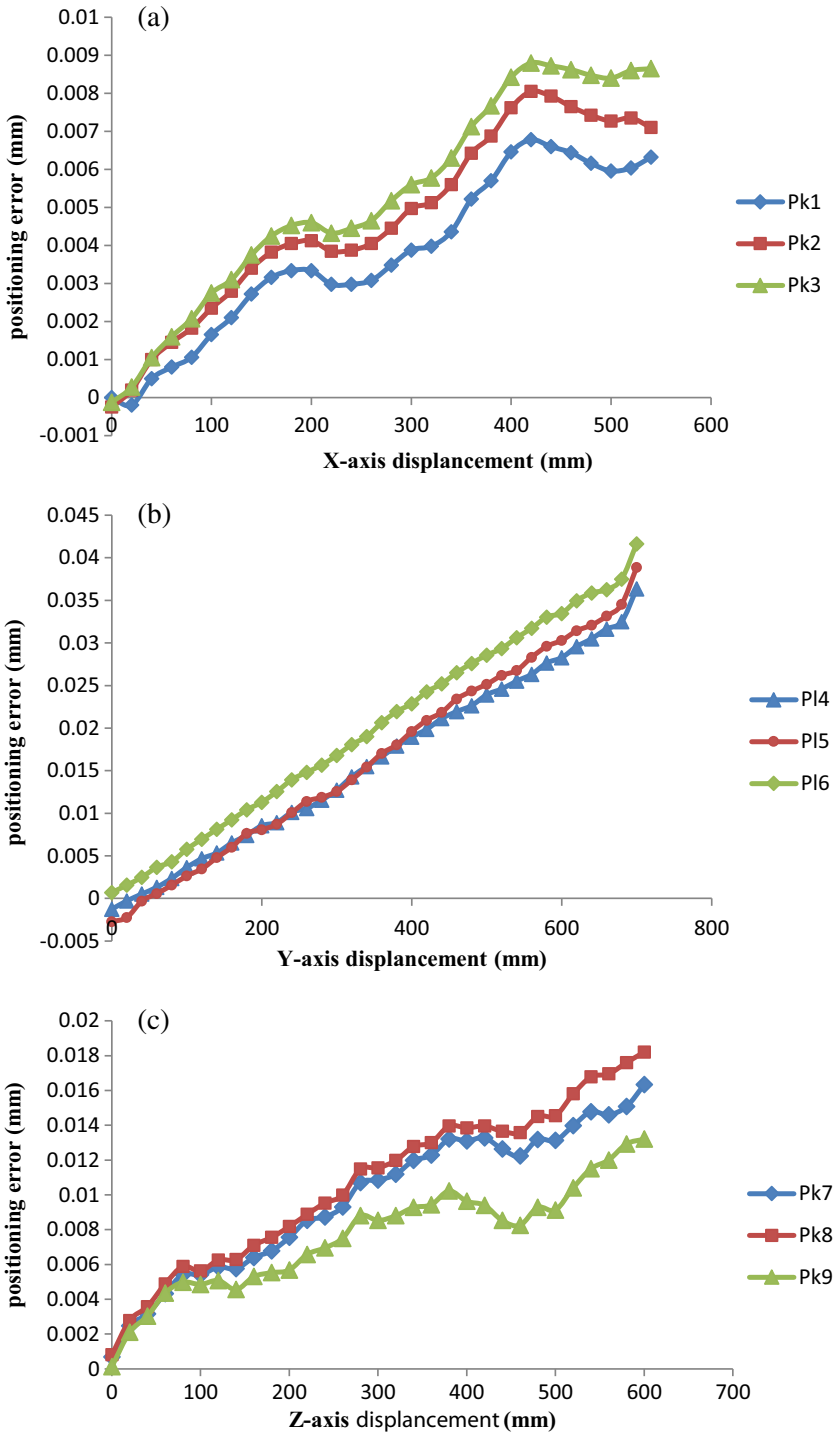

Fig. 12 The curve chart of the displacement and error in single-axis motion. **a** X axis. **b** Y axis. **c** Z axis

(1) Construct the polynomial equation, which can be expressed by

$$Y = X^T \beta \tag{48}$$

where $Y = (Y_1 \ \ Y_2 \ \cdots \ Y_h)^T$, $\beta = (\beta_1 \ \ \beta_2 \ \cdots \ \beta_p)^T$, $Y_j = B_{ij}$, and $Y_j = \sum_{i=1}^{p} X_{ij}\beta_i$ $(j = 1, 2, \cdots h)$. β denotes the coefficient matrix in Eq. (48).

(2) Obtain the values of β based on the method discussed in Sect. 4.2.

(3) Test the significance of Eq. (48) by F test [40]. The significance level α is usually chosen as 0.05. If the test result, i.e., P value, is higher than α, the significance test of the equation cannot be passed. In other words, the polynomial equation cannot describe the PDGE. On the contrary, the polynomial is suitable for the error. At this point, we should continue to the next step.

Table 5 The coordinate of measurement points in two-axis synchronous motion (unit: mm)

Motion pattern	Measurement point			Coordinate system
XZ axis linkage	P_{k1}	$r_{k1}(r_{k1x}, r_{k1y}, r_{k1z})$	(−75.2, 31.8, 58.3)	TCS
	P_{k2}	$r_{k2}(r_{k2x}, r_{k2y}, r_{k2z})$	(−75.2, 81.7, 58.3)	TCS
XY axis linkage	P_1	$r_{l1}(r_{l1x}, r_{l1y}, r_{l1z})$	(130, 195, 75)	WCS
		$r_{k1}(r_{k1x}, r_{k1y}, r_{k1z})$	(−187.8, 97, −49.127)	TCS
	P_2	$r_{l2}(r_{l2x}, r_{l2y}, r_{l2z})$	(130, 195, 105)	WCS
		$r_{k2}(r_{k2x}, r_{k2y}, r_{k2z})$	(−187.8, 97, −19.127)	TCS
YZ axis linkage	p_1	$r_{l1}(r_{l1x}, r_{l1y}, r_{l1z})$	(113, 20, 78)	WCS
		$r_{k1}(r_{k1x}, r_{k1y}, r_{k1z})$	(−220, 93, −26)	TCS

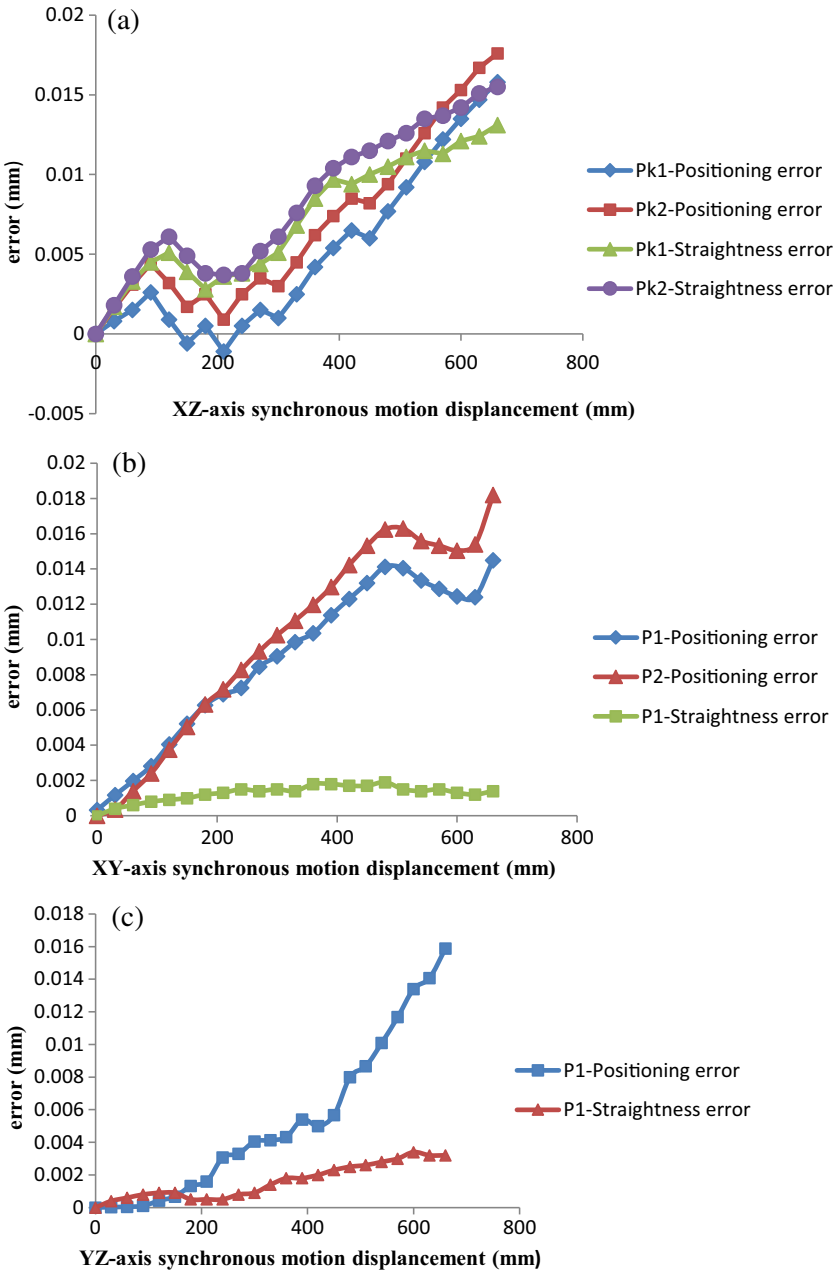

Fig. 13 The curve chart of the displacement and error in multi-axis synchronous motion. **a** *XZ* axis. **b** *XY* axis. **c** *YZ* axis

Table 6 The three PIGE values of three translational axes (unit: rad)

ε_{xy}	ε_{xz}	ε_{yz}
− 0.000005	0.000026	0.00001

(4) Determine whether X has any effect on Y. At first, the significance test of $\beta_i(i = 1, 2, \cdots p)$ based on t test [41] is carried out. If each P value calculated is less than the significance level α, the significance tests of β_i are considered as being passed. That means the established polynomial equation can perfectly represent the PDGE behavior. While if β_i do not pass the test, this shows that this equation has the redundant terms, which have little influence on the PDGE. Since Akaike information criterion (AIC) [42] can be used to weigh the goodness of fit of the polynomial, while the stepwise regression method [40] can be used to remove the least important terms, in this study, the stepwise regression method based on AIC is utilized to determine whether X has any effect on Y.

(5) The steps mentioned above are repeated until the significance tests of both the equation and β_i can be passed.

4.4 Fitting accuracy analysis

In this section, polynomial optimization is performed by R language 3.1.1 on a computer having a 3.10 GHz frequency. In this paper, for example, the polynomials of the pitch error for X axis can be represented on the basis of the least-squares method, as shown in Eq. (49).

$$\varepsilon_y(x) = 1.16302 \times 10^{-1}x - 1.43581 \times 10^{-3}x^2 + 8.16363 \times 10^{-6}x^3 - 2.21082 \times 10^{-8}x^4 + 2.76963 \times 10^{-11}x^5 - 1.15323 \times 10^{-14}x^6 - 2.13978 \times 10^{-18}x^7(\mu\text{rad}) \quad (49)$$

Then, Eq. (50) can be obtained by transforming Eq. (49)

$$\varepsilon_y(x) = 1.16302 \times 10^{-1}X_1 - 1.43581 \times 10^{-3}X_2 + 8.16363 \times 10^{-6}X_3 - 2.21082 \times 10^{-8}X_4 + 2.76963 \times 10^{-11}X_5 - 1.15323 \times 10^{-14}X_6 - 2.13978 \times 10^{-18}X_7(\mu\text{rad}) \quad (50)$$

where $X_i = x^i(i = 1, 2, \cdots 7)$.

Since the P value for Eq. (50) is 3.5341×10^{-21}, while the P values for $X_i(i = 1, 2, \cdots 7)$ are 3.91759×10^{-5}, 0.034867, 0.240908, 0.533366, 0.770712, 0.928049, and 0.974858, respectively, that means Eq. (50) has the redundant terms although it can describe the pitch error of X axis. According to Sect. 4.3, the following equation is obtained.

$$\varepsilon_y(x) = 8.22104 \times 10^{-2}X_1 - 6.40509 \times 10^{-4}X_2 + 1.87087 \times 10^{-6}X_3 - 7.44546 \times 10^{-12}X_5 + 7.93764 \times 10^{-15}X_6 \quad (51)$$

Herein, the P values for Eq. (51), X_1, X_2, X_3, X_5, X_6 are 1.19152×10^{-22}, 7.59006×10^{-10}, 1.45651×10^{-6}, 1.15052×10^{-5}, 8.80975×10^{-5}, and 1.76691×10^{-4}, respectively. Therefore, the optimal polynomial of the pitch error for X axis is obtained as follows.

$$\varepsilon_y(x) = 8.22104 \times 10^{-2}x - 6.40509 \times 10^{-4}x^2 + 1.87087 \times 10^{-6}x^3 - 7.44546 \times 10^{-12}x^5 + 7.93764 \times 10^{-15}x^6(\mu\text{rad}) \quad (52)$$

In the same way, the optimal polynomials of the rest PDGEs for three translational axes can also be represented.

As discussed above, the scatter diagram of discrete data and the polynomial curve diagram before and after optimization for the pitch error of X axis can be obtained, as shown in Fig. 14. According to Fig. 14, the fitting curve after optimization is closer to the discrete point than that before optimization. In order to demonstrate the goodness of fit of this

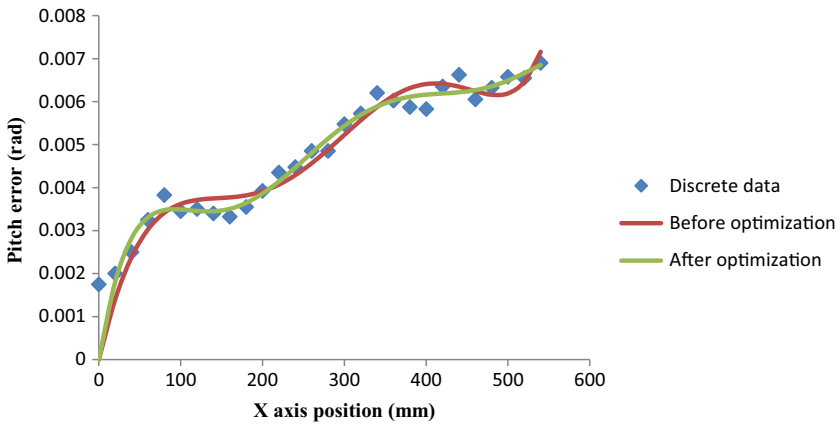

Fig. 14 The scatter diagram of discrete data and the polynomial curve diagram before and after optimization for the pitch error of X axis

optimization method, the comparison of some fitting parameters before and after optimization for the pitch error of X axis is shown in Fig. 15. According to Fig. 15, the term number and residual standard error of the polynomial before and after optimization are reduced from 7 to 5 and from 0.2836 to 0.2717, respectively, while adjusted R^2 before and after optimization, which is the number indicating data fitting degree, is increased from 0.9449 to 0.9474. This shows that the optimal method used in this paper possesses less term numbers, smaller fitting residuals, and higher fitting accuracy than the traditional methods. Hence, the prediction results of the polynomial can be directly used for software compensation.

5 Error compensation and results

5.1 The basic idea of error compensation

Suppose that the test path of tool ball is known in the identification process of the rotary axes' geometric errors. If the rotary axes keep still, the motion path variation can be considered as being caused simply by geometric errors of the translational axes. In our last research [43], an iterative compensation methodology for geometric errors of five axes in a machine tool was developed. The influence of geometric errors for the translational axes on the machine tool is not considered. As a matter of fact, this paper is an extended application for ref. [43] to improve the machining accuracy of the machine tool by eliminating the influence of the translational axes' errors on the rotary ones.

According to Sect. 2, suppose that the position array of P_T and P_W in MCS is written as P_T^M and p_W^M, respectively. In addition, ignoring geometric errors, the ideal position array of P_T^W can be written as $P_{Ti\ deal}^W$. So, the position vector of DBB P_D can be represented as follows.

$$P_D = P_T^M - P_W^M \tag{53}$$

where $P_T^M = [SBT]P_T, P_W^M = [SBW]P_W$.

According to the compensation method in ref. [10], to eliminate the influence of the translational axes' geometric errors on rotary ones, P_D should be coincident with the vector difference of $P_{T\ ideal}^W$ and P_W at any moment, as shown in Figs. 2 and 16. Therefore, Eq. (54) can be obtained.

$$P_D = P_T^M - P_W^M = P_{Ti\ deal}^W - P_W \tag{54}$$

For the convenience of description, the following equation can be denoted by simplifying Eq. (54).

$$\begin{bmatrix} x_T \\ y_T \\ z_T \\ 1 \end{bmatrix} = \Psi(x,y,z) = \begin{bmatrix} \Psi_x(x,y,z) \\ \Psi_y(x,y,z) \\ \Psi_z(x,y,z) \\ 1 \end{bmatrix} \tag{55}$$

where x_T, y_T, z_T denote the coordinate values of P_T, and x, y, z denote the NC code driving the movement of translational axes. The physical meaning of Eq. (55) is that the real position of tool ball can be calculated in real time by the given NC code.

Assume that the NC code of the test path for tool ball can be represented as (x_0, y_0, z_0) (namely, the ordinary compensation method). By using Eqs. (5), (6), and (55), the positioning errors of tool ball can be obtained. However, its positioning accuracy cannot meet the actual accuracy requirements. As a result, an iterative compensation is essential, as shown in Fig. 17. Based on Eq. (6), until E satisfies Eq.(56), the iterative compensation is not

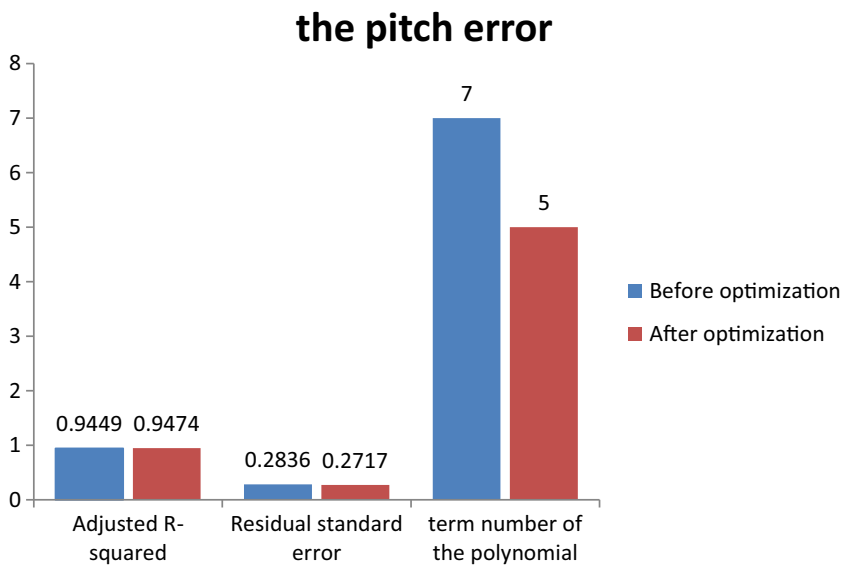

Fig. 15 The comparison of some fitting parameters before and after optimization for the pitch error of X axis

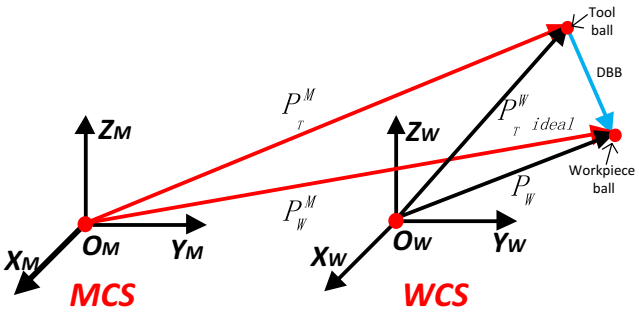

Fig. 16 The schematic diagram of the coordinate system transformation

terminated. Thus, the modified NC code (x_n, y_n, z_n) of the test path for tool ball is obtained.

$$E \leq \Delta_{\mathrm{DBB}} \tag{56}$$

where Δ_{DBB} denotes the resolution of the DBB. In this study, $\Delta_{\mathrm{DBB}} = 0.001$ (mm).

In order to carry out the iterative compensation method, error compensation software is developed. Please note that the modified NC codes generated in this way can be used to drive the translational axes of the MAMT in real time during the DBB test so as to avoid the influence of the translational axes' geometric errors on rotary ones and improve the positioning accuracy of tool ball.

5.2 Simulation verification of error compensation

To verify the effectiveness of the proposed method, simulation is conducted on a five-axis machine tool, as shown in Fig. 1a. The simulation mainly includes two parts: (1) the positioning errors of tool ball are computed with the ordinary compensation method, and (2) the positioning errors of tool ball are computed

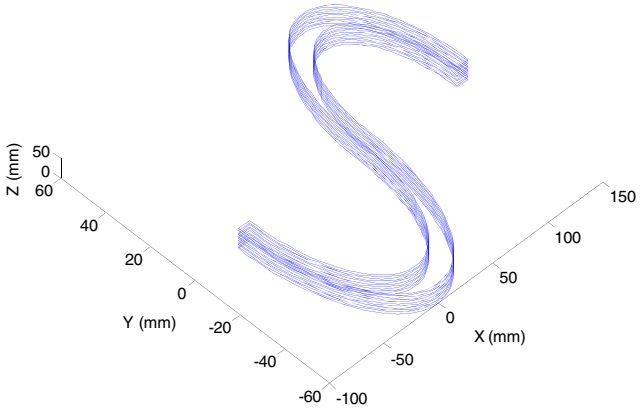

Fig. 18 Test path of cutting tool end

with the iterative compensation method. According to Sect. 4, PDGEs of the translational axes are predicted in real time at any position. So they are not described here. Test path planning of tool ball in this paper is put into effect by Pro/E software based on the path like the letter S, as shown in Fig. 18. Then, the cutter location source file (CLSF) is generated by the post process module of Pro/E software.

Based on CLSF, the NC codes with these two methods are generated in self-developed compensation software, respectively. Then, their positioning errors are calculated. The error maps generated with these two NC codes are drawn in Fig. 19. In order to further reflect the average state and the stability of positioning accuracy, the expectation and standard deviation of positioning errors also should be taken into account, as shown in Fig. 20.

From Fig. 19a, it can be seen that the maximum value of positioning errors calculated with the ordinary compensation method is 0.0021 mm, which cannot meet the requirement of

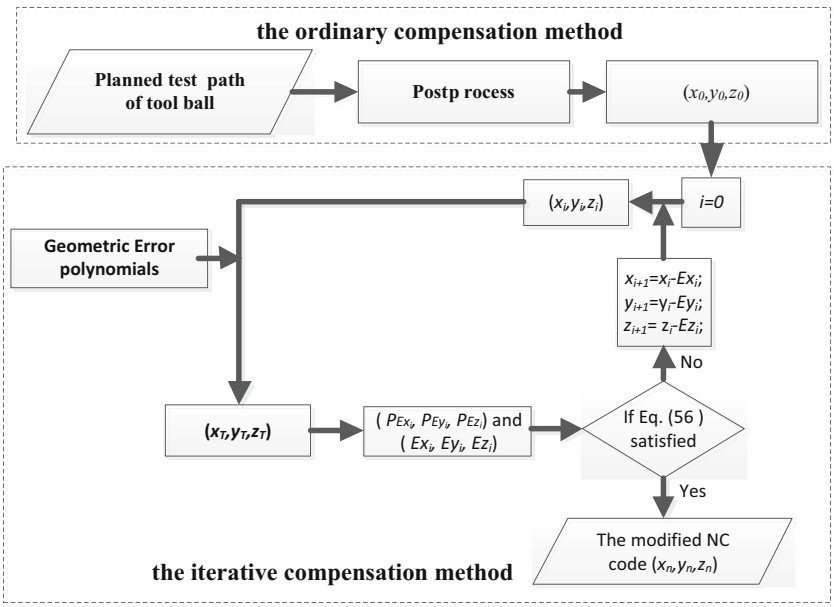

Fig. 17 The flow chart of error compensation

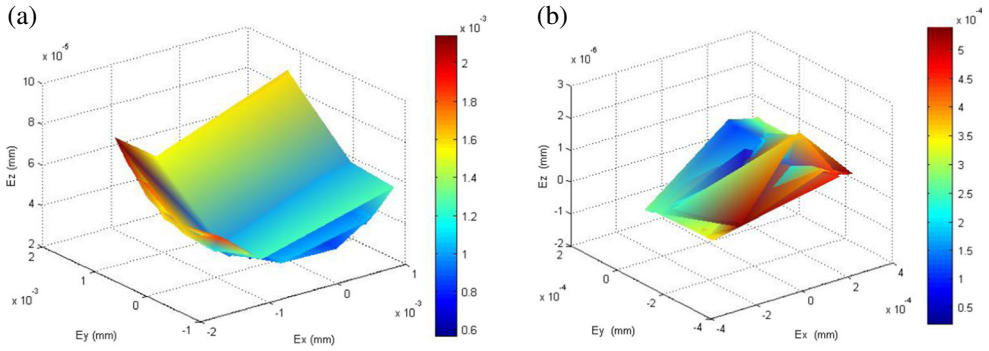

Fig. 19 The positioning error maps with two compensation methods. **a** The ordinary compensation method. **b** The iterative compensation method

positioning accuracy for tool ball. Since the resolution of the DBB is usually 0.001 mm, there is no doubt that the errors of translational axes cannot be fully compensated and the residuals actually still have some influence on the DBB.

After applying the iterative compensation method, the maximum positioning error is 0.00053 mm, as shown in Fig. 19b. In other words, the positioning errors with the iterative compensation method, which is limited within 0.001 mm, have no influence on the DBB. Based on Fig. 20, the average accuracy and the standard deviation of positioning errors are 0.00119 and 0.000249 mm before compensation and 0.000244 and 0.000119 mm after compensation, respectively. The total accuracy and accuracy stability of positioning errors have been improved by 79.5 and 52.2%, respectively. Therefore, a conclusion can be drawn that the proposed method in this paper can efficiently eliminate the influence of the translational axes' geometric errors on rotary axes.

5.3 Experiment test results

In order to further verity the feasibility of the presented method, a test experiment is conducted on a five-axis machine tool (as mentioned in Sect. 4). Test conditions of the experiment are shown in Table 7. Before the test, the DBB must be calibrated. Then, its two ends are carefully mounted on the spindle and the worktable of the machine tool, respectively, as shown in Fig. 21.

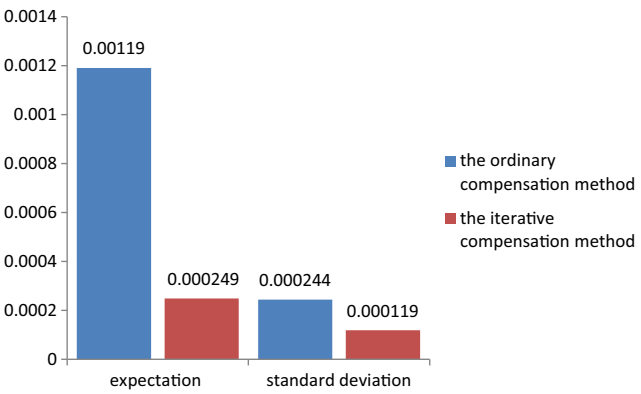

Fig. 20 Expectation and standard deviation of positioning errors

According to Sect. 5.2, these two NC codes generated with the ordinary compensation method and the iterative compensation method are used to drive the translational axes of the five-axis machine tool, respectively. Then, these two circular trajectories formed by multi-axis motion in *XY* plane are measured by using a DBB, QC20-W by Renishaw. The measuring result charts of DBB in *XY* plane with these two methods are displayed in Fig. 22. According to Fig. 22, their maximum circularity errors can be obtained. The comparison of the maximum circularity error with these two methods is shown in Table 8.

As can be seen in Table 8, the maximum circularity error with the ordinary compensation method is 42.1 μm. And the maximum circularity error with the iterative compensation method is 25.1 μm. In other words, the error reduction by using the iterative compensation method is about 40.4%. Therefore, it is obvious that the proposed compensation method in this paper is more precise and effective than the ordinary compensation method.

It is important to note that the experiment results are little worse than the simulation results. It is because that many other error sources, dynamitic errors, control errors, thermal errors, and so on, can affect the compensation effect. Anyway, the core idea of the method can be applied for the positioning accuracy improvement of tool ball for DBB.

6 Conclusions

In this paper, an integrated geometric error prediction and compensation method is proposed to eliminate the positioning inaccuracy of tool ball for a double bar ball (DBB) caused by the translational axes' geometric errors in a multi-axis machine tool (MAMT). For the sake of the effective implementation of the method, firstly, the positioning error model only considering the translational axes of FAMT is established. By using this model, the positioning accuracy of tool ball can be predicted.

Table 7 Test conditions in the experiment

	Test specification	Test plane	Ball bar length (mm)	Feed rate (mm/min)	Sample rate (HZ)	Run direction	Test temperature (°)
Test parameter	*XY* 360° 300 mm	*XY*	300.0000	1000.0	13.333		
Run 1						Clockwise	20
Run 2						Counterclockwise	20

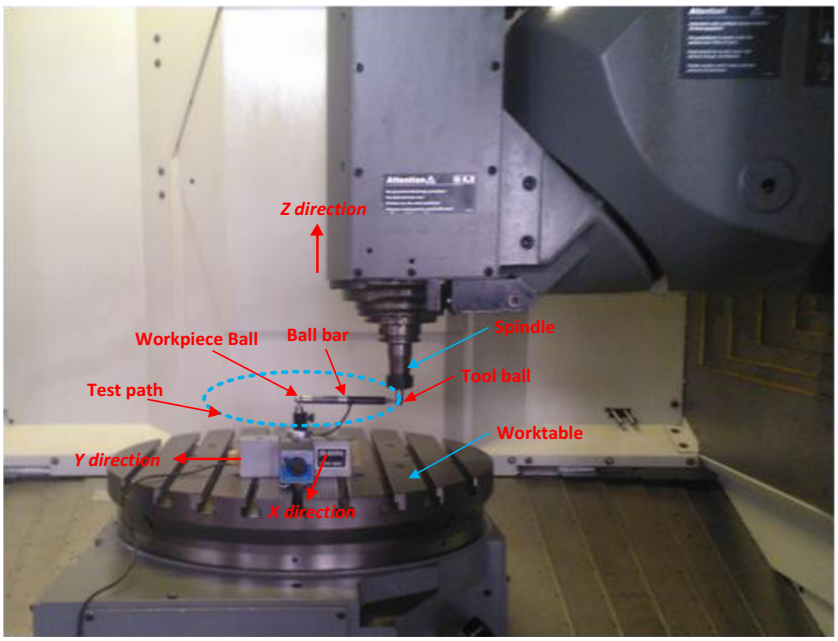

Fig. 21 The measuring scenes of the DBB in *XY* plane

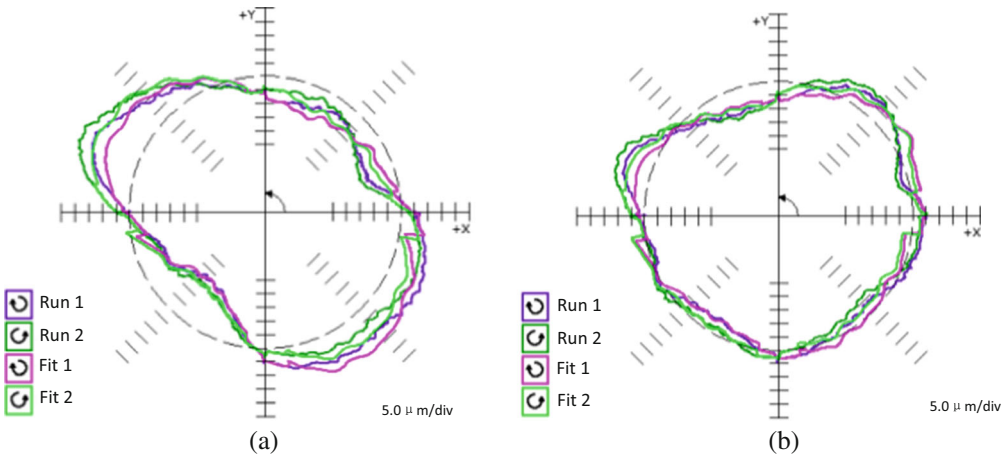

Fig. 22 The measuring result charts of the DBB in *XY* plane with two methods. **a** The ordinary compensation method. **b** The iterative compensation method

Table 8 The comparison of the maximum circularity error

The maximum circularity error (μm)		Error reduction (%)
The ordinary compensation method	The iterative compensation method	
42.1	25.1	40.4

Then, to obtain the translational axes' geometric errors, an integrated error parameter identification method (IEPIM) is proposed. Compared with the previous identification methods, the IEPIM has the advantages, such as higher identification speed and accuracy, stronger applicability and generality, and easier realization of computer automatic programming, and so on, which lays a foundation for software error compensation. In addition, by identification experiments, the identification results of geometric error parameters for the translational axes are obtained. In order to predict the positioning error at an arbitrary position effectively, the optimal polynomials of 18 position-dependent geometric errors (PDGEs) are founded based on their discrete values. By fitting accuracy analysis, these models possess less term numbers, smaller fitting residuals, and higher fitting accuracy than the traditional methods. This means that the optimal models of geometric errors are more suitable for software compensation.

Finally, simulation verification is conducted. Simulation results show that the maximum positioning error for test path of tool ball with the ordinary compensation method is 0.0021 mm and the maximum positioning error with the iterative compensation method is 0.00053 mm. Furthermore, the average accuracy and the standard deviation of positioning errors are 0.00119 and 0.000249 mm with the ordinary compensation method and 0.000244 and 0.000119 mm with the iterative compensation method, respectively. The total accuracy and accuracy stability of positioning errors has been improved by 79.5 and 52.2%, respectively. In order to further verity the feasibility of the presented method, a measuring experiment is conducted in *XY* plane of a five-axis machine tool by using a DBB. The experiment results show that the maximum circularity error with the iterative compensation method is reduced about 40.4% than that with the ordinary compensation method. According to the simulation and experiment results, the proposed method in this paper is more precise and efficient than the ordinary compensation method, seen in the ref. [43] for instance. Therefore, there is no doubt that the method can effectively avoid the influence of the translational axes' geometric errors on rotary ones during a DBB test. Thus, this work will provide an important guidance for researchers and practicing engineers in the field of machine tool to eliminate the influence of the translational axes' errors on the rotary ones.

However, this paper is mainly concentrated on compensating the geometric errors of the machine tool. A further study should be conducted in the future to consider all of error sources or at least most of them.

Funding information This work is financially supported by the National Natural Science Foundation of China (Nos. 51775010 and 51705011) and the Science and Technology Major Projects of High-end CNC Machine Tools and Basic Manufacturing Equipment of China (No. 2014ZX04011031). The authors appreciate the support from the Key Scientific Research Project for Henan Province Higher School of China (No. 18A460036).

References

1. Khan AW, Chen W (2010) A methodology for error characterization and quantification in rotary joints of multi-axis machine tools. Int J Adv Manuf Technol 51(9–12):1009–1022. https://doi.org/10.1007/s00170-010-2677-4
2. Zhu J (2008) Robust thermal error modeling and compensation for CNC machine tools[D]. University of Michigan, Ann Arbor
3. Chen D, Dong L, Bian Y, Fan J (2015) Prediction and identification of rotary axes error of non-orthogonal five-axis machine tool. Int J Mach Tool Manu 94:74–87. https://doi.org/10.1016/j.ijmachtools.2015.03.010
4. Ramesh R, Mannan MA, Poo AN (2000) Error compensation in machine tools—a review part I: geometric, cutting-force induced and fixture-dependent errors. Int J Mach Tools Manuf 40(9):1235–1256. https://doi.org/10.1016/S0890-6955(00)00009-2
5. Tsutsumi M, Saito A (2003) Identification and compensation of systematic deviations particular to 5-axis machining centers. Int J Mach Tools Manuf 43(8):771–780. https://doi.org/10.1016/S0890-6955(03)00053-1
6. Lee K II, Lee D-M, Yang S-H (2012) Parametric modeling and estimation of geometric errors for a rotary axis using double ballbar. Int J Adv Manuf Technol 62(5–8):741–750. https://doi.org/10.1007/s00170-011-3834-0
7. Lee K II, Yang S-H (2013) Measurement and verification of position-independent geometric errors of a five-axis machine tool using a double ball-bar. Int J Mach Tool Manu 70:45–52. https://doi.org/10.1016/j.ijmachtools.2013.03.010
8. Chen J, Lin S, Zhou X, Gu T (2016) A ballbar test for measurement and identification the comprehensive error of tilt table. Int J Mach Tool Manu 103:1–12. https://doi.org/10.1016/j.ijmachtools.2015.12.002
9. Xiang S, Yang J, Zhang Y (2014) Using a double ball bar to identify position-independent geometric errors on the rotary axes of five-axis machine tools. Int J Adv Manuf Technol 70(9–12):2071–2082. https://doi.org/10.1007/s00170-013-5432-9
10. Hsu YY, Wang SS (2007) A new compensation method for geometry errors of five-axis machine tools. Int J Mach Tool Manu 47(2):352–360. https://doi.org/10.1016/j.ijmachtools.2006.03.008
11. Zhang H, Yang J, Zhang Y, Shen J, Wang C (2011) Measurement and compensation for volumetric positioning errors of CNC machine tools considering thermal effect. Int J Adv Manuf Technol 55(1–4):275–283. https://doi.org/10.1007/s00170-010-3024-5
12. Schwenke H, Knapp W, Haitjema H, Weckenmann A, Schmitte R, Delbressine F (2008) Geometric error measurement and compensation of machines-an update. CIRP Ann Manuf Technol 57(2):660–675. https://doi.org/10.1016/j.cirp.2008.09.008
13. Ibaraki S, Knapp W (2012) Indirect measurement of volumetric accuracy for three-axis and five-axis machine tools: a review. Int J Autom Technol 6(2):110–124. 10.20965/ijat.2012.p0110
14. Du S, Hu J, Yu Z, Hu C (2017) Analysis and compensation of synchronous measurement error for multi-channel laser interferometer. Meas Sci Technol 28(5):055201–055207
15. Ngoi BKA, Chin CS (2000) Self-compensated heterodyne laser interferometer. Int J Adv Manuf Technol 16(3):217–219
16. Zhang G, Lu B, Ouyang R, Hocken R, Veale R, Donmez A (1988) A displacement method for machine geometry calibration. CIRP Ann Manuf Technol 37(1):515–518. https://doi.org/10.1016/S0007-8506(07)61690-4
17. Liu YW, Liu LB, Zhao XS, Zhang Q, Wang SX (1998) Investigation of error compensation technology for NC machine tool. China J Mech Eng 9(12):48–52 (in Chinese)

18. Fan J, Tian Y, Song G, Huang X, Kang C (2000) Technology of NC machine error parameter identification based on fourteen displacement measurement line. J Beijing Polytech Univ, China 26(6):11–15 (in Chinese)
19. Chen G, Yuan J, Ni J (2001) A displacement measurement approach for machine geometric error assessment. Int J Mach Tool Manu 41(1):149–161. https://doi.org/10.1016/S0890-6955(00)00049-3
20. Su S, Li S, Wang G (2002) Identification method for errors of machining center based on volumetric error model. Chin J Mech Eng 38(7):121–125 (in Chinese)
21. Li J, Xie F, Liu XJ, Li W, Zhu S (2016) Geometric error identification and compensation of linear axes based on a novel 13-line method. Int J Adv Manuf Technol 87(5–8):2269–2283. https://doi.org/10.1007/s00170-016-8580-x
22. Cui G, Lu Y, Li J, Gao D, Yao Y (2012) Geometric error compensation software system for CNC machine tools based on NC program reconstructing. Int J Adv Manuf Technol 63(1–4):169–180. https://doi.org/10.1007/s00170-011-3895-0
23. Ding S, Huang X, Yu C, Liu X (2016) Novel method for position-independent geometric error compensation of five-axis orthogonal machine tool based on error motion. Int J Adv Manuf Technol 83(5–8):1069–1078. https://doi.org/10.1007/s00170-015-7642-9
24. Khan AW, Chen W (2011) A methodology for systematic geometric error compensation in five-axis machine tools. Int J Adv Manuf Technol 53(5–8):615–628. https://doi.org/10.1007/s00170-010-2848-3
25. Chen J, Lin S, He B (2014) Geometric error compensation for multi-axis CNC machines based on differential transformation. Int J Adv Manuf Technol 71(1–4):635–642. https://doi.org/10.1007/s00170-013-5487-7
26. Cheng Q, Zhao H, Zhang G, Gu P, Cai L (2014) An analytical approach for crucial geometric errors identification of multi-axis machine tool based on global sensitivity analysis. Int J Adv Manuf Technol 75(1–4):107–121. https://doi.org/10.1007/s00170-014-6133-8
27. Guo S, Zhang D, Xi Y (2016) Global quantitative sensitivity analysis and compensation of geometric errors of CNC machine tool. Math Probl Eng 2016:1–12
28. Cheng Q, Zhang Z, Zhang G, Gu P, Cai L (2015) Geometric accuracy allocation for multi-axis CNC machine tools based on sensitivity analysis and reliability theory. Proc IMechE C J Mech Eng Sci 229(6):1134–1149. https://doi.org/10.1177/0954406214542491
29. Fan JW, Guan JL, Wang WC, Luo Q, Zhang XL, Wang LY (2002) A universal modeling method for enhancement the volumetric accuracy of CNC machine tools. J Mater Process Technol 129(1–3):624–628. https://doi.org/10.1016/S0924-0136(02)00669-6
30. Zhu S, Ding G, Qin S, Lei J, Zhang L, Yan K (2012) Integrated geometric error modeling, identification and compensation of CNC machine tools. Int J Mach Tool Manu 52(1):24–29. https://doi.org/10.1016/j.ijmachtools.2011.08.011
31. He Z, Fu J, Zhang X, Shen H (2016) A uniform expression model for volumetric errors of machine tools. Int J Mach Tool Manu 100:93–104. https://doi.org/10.1016/j.ijmachtools.2015.10.007
32. Jung J-H, Choi J-P, Lee S-J (2006) Machining accuracy enhancement by compensating for volumetric errors of a machine tool and on-machine measurement. J Mater Process Technol 174(1–3):56–66. https://doi.org/10.1016/j.jmatprotec.2004.12.014
33. Bringmann B, Besuchet JP, Rohr L (2008) Systematic evaluation of calibration methods. CIRP Ann Manuf Technol 57(1):529–532. https://doi.org/10.1016/j.cirp.2008.03.114
34. Lasemi A, Xue D, Gu P (2016) Accurate identification and compensation of geometric errors of 5-axis CNC machine tools using double ball bar. Meas Sci Technol 27(5):055004–055021. https://doi.org/10.1088/0957-0233/27/5/055004
35. Huang N, Jin Y, Bi Q (2015) Integrated post-processor for 5-axis machine tools with geometric errors compensation. Int J Mach Tool Manu 94:65–73. https://doi.org/10.1016/j.ijmachtools.2015.04.005
36. Lee J-H, Liu Y, Yang S-H (2006) Accuracy improvement of miniaturized machine tool: geometric error modeling and compensation. Int J Mach Tool Manu 46(12-13):1508–1516. https://doi.org/10.1016/j.ijmachtools.2005.09.004
37. Cheng Q, Wu C, Peihua G, Chang W, Xuan D (2013) An analysis methodology for stochastic characteristic of volumetric error in multiaxis CNC machine tool. Math Probl Eng 2013:1–12
38. Lee K II, Yang S-H (2013) Robust measurement method and uncertainty analysis for position-independent geometric errors of a rotary axis using a double ball-bar. Int J Precis Eng Manuf 14(2):231–239. https://doi.org/10.1007/s12541-013-0032-z
39. ISO 230-1 (2012) Test code for machine tools—part 1: geometric accuracy of machines operating under no-load or quasi-static conditions 1–11
40. Sharma MJ, Jin YS (2015) Stepwise regression data envelopment analysis for variable reduction. Appl Math Comput 253:126–134
41. Liu Y, Fan J, Miao W (2013) Soft compensation for CNC crankshaft grinding machine tool. Adv Mech Eng 2013:1–11
42. Akaike H (1978) A Bayesian analysis of the minimum AIC procedure. Ann Inst Stat Math 30(1):9–14. https://doi.org/10.1007/BF02480194
43. Wu C, Fan J, Wang Q, Chen D (2018) Machining accuracy improvement of non-orthogonal five-axis machine tools by a new iterative compensation methodology based on the relative motion constraint equation. Int J Mach Tools Manuf 124(1):80–98. https://doi.org/10.1016/j.ijmachtools.2017.07.008